

JGR Earth Surface

RESEARCH ARTICLE

10.1029/2019JF005060

Key Points:

- River inundation causes permafrost warming and rapid subsurface thaw front deepening
- Increasing Arctic river discharge leads to the expansion of channelbed thaw bulbs and degradation of floodplain permafrost
- Shifts in the timing of onset of river flooding are more impactful for permafrost warming than a prolonged warm season

Supporting Information:

- Supporting Information S1
- · Animation S1
- · Animation S2

Correspondence to:

I. Overeem, irina.overeem@colorado.edu

Citation:

Zheng, L., Overeem, I., Wang, K., & Clow, G. D. (2019). Changing Arctic River dynamics cause localized permafrost thaw. *Journal of Geophysical Research: Earth Surface*, 124, 2324–2344. https://doi.org/10.1029/2019JF005060

Received 6 MAR 2019 Accepted 30 AUG 2019 Accepted article online 4 SEP 2019 Published online 10 SEP 2019

Changing Arctic River Dynamics Cause Localized Permafrost Thaw

Lei Zheng^{1,2} D, Irina Overeem^{1,3} D, Kang Wang¹ D, and Gary D. Clow¹ D

¹CSDMS, Institute of Arctic and Alpine Research, University of Colorado Boulder, Boulder, CO, USA, ²Chinese Antarctic Center of Surveying and Mapping, Wuhan University, Wuhan, China, ³Department of Geological Sciences, University of Colorado Boulder, Boulder, CO, USA

Abstract Permafrost in the Arctic regions is degrading in response to decades of amplified warming. Advanced degradation of ice-rich permafrost could significantly alter the water balance by increasing runoff and flooding. How do the hydrological changes in river systems, in turn, affect the permafrost thermal state, specifically in floodplains? First, we develop a first-order heat budget approach to simulate evolving river-water temperature. The river-water thermal model includes heat exchanges at both the air-water and water-subsurface interfaces and can accurately estimate water temperature. Then, river-water temperature is employed as an upper boundary condition for the control volume permafrost model, which models the thermal state of shallow permafrost. The combined model is validated and applied in the Kuparuk River floodplain, Alaska. Results indicate that permafrost warms rapidly during inundation and that channelbelt active layer thickness can deepen by more than 1 m. We find that earlier arrival of the spring freshet and associated earlier inundation onset, as well as increase in river discharge, can significantly increase subsurface permafrost temperature and lead to a deepening of the active layer. In recent years Kuparuk River streamflow has arrived earlier, and mean annual river discharge has increased by 35% since the 1970s. New permanent water and seasonal water appeared throughout the river network of the Kuparuk River since the 1980s according to satellite observations. These hydrological changes likely have contributed to the expansion of riverbed thaw bulbs and the degradation of floodplain permafrost.

1. Introduction

Globally, the average surface temperature increased 0.85 °C during 1880–2012 (Stocker et al., 2013), yet the Arctic has warmed more than twice as fast as the global average (Cohen et al., 2014; Polyakov et al., 2002), leading to the dramatic melting of sea ice, glaciers, and snow cover, as well as permafrost degradation (Serreze & Stroeve, 2015; Stocker et al., 2013; Zhang et al., 2005). Permafrost, the area with soil temperatures that remain below 0 °C for at least two consecutive years, underlies approximately 24% of the exposed land area of the Northern Hemisphere (Zhang et al., 1999). Climatic change has resulted in an increase of permafrost temperature, a decrease of permafrost extent, and deepening of the active layer across the Arctic during the past half century (Streletskiy et al., 2015). Arctic hydrology also exhibited extensive responses to climate warming. Land-based ice melt, precipitation, and river runoff are all increasing under the current climatic trends (AMAP, 2017; McClelland et al., 2006; Overeem & Syvitski, 2010; Pavelsky & Zarnetske, 2017; Peterson et al., 2002), resulting in an increased freshwater volume draining into the Arctic Ocean (Haine et al., 2015).

Strong interactions are to be expected between Arctic permafrost and hydrological processes. Alterations in the permafrost conditions can impact the hydrological system through surface infiltration, soil drainage, and subsurface flow, leading to changes in groundwater dynamics and surface runoff (Yamazaki et al., 2006; Walvoord et al., 2012; T. M. Jorgenson et al., 2013; Koch et al., 2013; Walvoord & Kurylyk, 2016; Evans & Ge, 2017). Permafrost degradation will trigger increasing interactions between surface and groundwater water, as well as changes in water storage (Lamontagne-Hallé et al., 2018; Walvoord & Striegl, 2007). In discontinuous permafrost regions, increased hydrogeologic connectivity results in more groundwater that flows to the downgradient river (Lamontagne-Hallé et al., 2018). Enhanced surface-groundwater interactions could also lead to the loss of lake water and the shrinking of lakes (Chen et al., 2013; Li et al., 2013; Nitze et al., 2017). As a consequence, the Arctic terrestrial fresh water system under continued permafrost thaw will likely transform from a surface-water-dominated system to a groundwater-dominated system in many

©2019. American Geophysical Union. All Rights Reserved.



areas of the Arctic (Frey & McClelland, 2009). Thawing ice-rich permafrost has the potential to increase sediment loads and alter geochemistry of streams, affecting water quality and even the river biota (Chin et al., 2016; Kokelj et al., 2013; Rudy et al., 2017).

Changes in hydrological processes, in turn, can profoundly affect permafrost conditions. Natural evolution and drainage of thaw lakes significantly disturb permafrost thermal state (Ling, 2004; Matell et al., 2013). Presence of groundwater flow may reduce permafrost thickness and enhance permafrost degradation (Mckenzie & Voss, 2013; Rowland et al., 2011). Flooding and inundation of the floodplain provide input of heat into the subsurface that warms the frozen ground. In addition, significant flood deposition of sand and silt on the floodplain impacts vegetation, preventing the formation of an insulating organic layer and thereby enhancing the warming of the underlying permafrost and the deepening of the active layer (Jorgenson et al., 1998; Viereck, 1973). Occasional or annual river inundation can prevent the development of permafrost beneath the riverbed (Brosten et al., 2009; Viereck, 1970). The depths of thaw bulbs beneath Arctic streams have been found to increase from the channel edges to the middle of a river (Bradford et al., 2005; Brosten et al., 2006). Warm flood water transfers heat into soil, leading to the increase of soil temperature or even the thawing of existing permafrost beneath the river floodplains in interior Alaska (Viereck, 1973).

Current understanding of the complex interactions between climate, permafrost, and hydrology remains inadequate due to the lack of climatic and hydrometric measurements in cold regions (Woo et al., 2008). Here, we ask how permafrost conditions are different within floodplain corridors as compared to the surrounding environment. Together with earlier snowmelt (AMAP, 2017; Tan et al., 2011), Arctic rivers have exhibited trends toward earlier river breakup and later river freezeup dates, reduced ice-cover duration, and increasing discharge and water temperature (Magnuson et al., 2000; Overeem & Syvitski, 2010; Park et al., 2017; Pavelsky & Zarnetske, 2017). Projected changes in the timing and magnitude of snowmelt runoff and the Arctic river-ice conditions may result in earlier timing of flood inundation and possibly affect further downstream river reaches (AMAP, 2017). How do these changes in timing and magnitude of river inundation impact the floodplain and delta plain permafrost conditions?

Here, we seek to understand how Arctic river inundation affects permafrost thermal state. Specifically, we develop a first-order approach to simulate evolving river-water temperature over the inundation period. Then, river temperature is employed as the upper temperature boundary condition in a permafrost model, which predicts the thermal state of the shallow subsurface permafrost. Our combined model is applied and validated for downstream reaches of the Kuparuk River, Arctic Alaska. Finally, we run simulations to investigate the response of permafrost temperatures and the active layer to changing flood timing and river discharge.

2. Methodology

Measurements of river water temperatures T_w are sparse, and when available, temperature is often discontinuously recorded in the Arctic region. To circumvent the data sparseness, we develop a one-dimensional heat-balance model to simulate T_w driven by atmospheric and hydrologic observations. Over the inundation period, T_w is substituted for the "dry land" ground surface temperatures T_g and serve as the upper boundary condition for a control volume permafrost model (CVPM; Clow, 2018a). We calculate permafrost temperature and active layer thickness (ALT) using CVPM. All model parameters are listed in Table 1.

2.1. River-Water Thermal Model

Our quantitative model of river temperature T_w is based on a heat budget approach (Figure 1). Heat fluxes considered in the model include net surface shortwave solar radiation (H_{sr}) , net longwave radiation (H_{lr}) , latent heat (H_l) due to evaporation and condensation, convective heat (H_c) , and riverbed heat flux (H_b) ; Hebert et al., 2011). With these terms, the net heat balance of the water body ΔH_w is

$$\Delta H_w = H_{sr} + H_{lr} + H_l + H_c + H_b. \tag{1}$$

Surface net solar radiation H_{sr} at the water surface is expressed as the direct solar irradiance penetrating the water surface, that is, the difference between incoming solar radiation (H_{is}) and reflected solar radiation (H_{rs}) , or

Table	1
Model	Parameters

No.	Parameter	Definition	Units		
1	H_{sr}	Surface net solar radiation	W/m ²		
2	H_{lr}	Surface net longwave radiation	W/m^2		
3	H_l	Surface latent heat	W/m^2		
4	H_c	Surface convective heat	W/m^2		
5	H_b	Riverbed heat flux	W/m^2		
6	H_{is}	Incoming solar radiation	W/m^2		
7	H_{rs}	Reflected solar radiation	W/m^2		
8	H_{dl}	Downward longwave radiation	W/m^2		
9	H_{el}	Emitted longwave radiation	W/m^2		
10	H_{w}	Net heat balance of the water body	W/m^2		
11	T_a	Surface air temperature	°C		
12	T_{g}	Ground surface temperature	°C		
13	T_s	Soil temperature	°C		
14	T_h	Temperature gradient of riverbed	°C/m		
15	U_w	Wind speed	m/s		
16	$\stackrel{\mathcal{O}_W}{P}$	Atmospheric pressure	mm Hg		
17	r	Relative humidity			
18	R	Water surface albedo			
19	e_{s}	Saturated vapor pressure at the water surface	mm Hg		
20		Atmospheric water vapor pressure	mm Hg		
21	$egin{array}{c} e_a \ \Sigma \end{array}$	Stefan-Boltzmann constant	$W/m^2 K^{-4}$		
22	a	Fraction of radiation absorbed in water	W/III K		
23	b	Fraction of radiation absorbed in riverbed	_		
		Attenuation coefficient	 m ⁻¹		
24	f_{l}				
25	h	Water depth	M		
26	z	Soil depth	M		
27	t	Time	Day		
28	$ ho_w$	Density of water	kg/m ³ J⋅kg ⁻¹ ⋅°C ⁻¹		
29	c_w	Heat capacity of water			
30	L	Soil depth of zero annual amplitude	m		
31	T_c	Soil temperature at L	°C W·m ⁻¹ ·°C ⁻¹		
32	$k_{\scriptscriptstyle S}$	Thermal conductivity of mineral grains			
33	$ ho_{\scriptscriptstyle S}$	Density of mineral grains	kg/m ³		
34	c_s	Heat capacity of mineral grains	$J \cdot kg^{-1} \cdot {}^{\circ}C^{-1}$		
35	S_0	Heat-production rate extrapolated to surface	$mW m^{-3}$		
36	$h_{\scriptscriptstyle S}$	Heat-production length scale	km		
37	Φ_0	Porosity extrapolated to surface	_		
38	Φ_c	Critical porosity	_		
39	h_c	Compaction length scale	km		
40	S_r	Degree of pore saturation	_		
41	x_s^*	Mole fraction of solutes extrapolated to zero ice			
42	λ	Interfacial melting parameter	$\mu m K^{1/3}$		
43	d_1	Effective diameter of larger mode pores	μm		
44	d_2	Effective diameter of smaller mode pores	μm		
45	n_2/n_1	Number of small pores/number of large pores	_		
46	Q	Discharge	m^3/s		
47	S	River stage	m		
48	G	Gauge height	m		
49	G_0	Gauge height offset	m		

$$H_{sr} = H_{is} - H_{rs} = (1 - R)H_{is},$$
 (2)

where R represents the water surface albedo.

Longwave radiation includes the radiation emitted by the atmosphere, water surface, and vegetation. We assume the vegetation canopy effect is negligible for the northernmost Arctic river floodplains. Net longwave radiation H_{lr} at the water surface is then the difference between atmospheric downward longwave radiation (H_{dl}) and the longwave radiation emitted from the water surface (H_{el}) ,

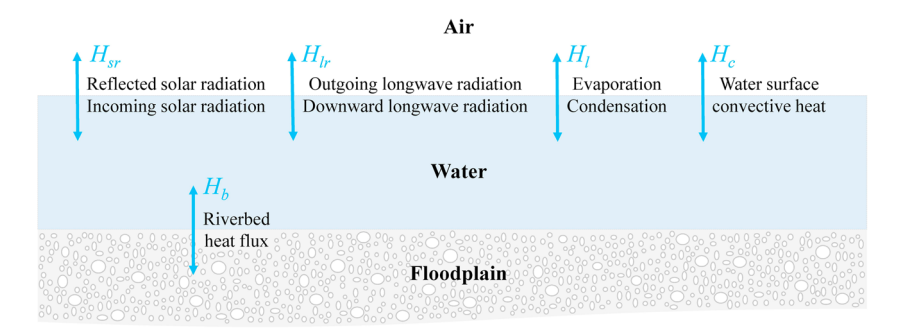


Figure 1. Schematic of the river water heat budget model.

$$H_{lr} = H_{dl} - H_{el}. (3)$$

The emitted longwave H_{el} can be calculated using the Stefan-Boltzmann Law (Gao & Merrick, 1996) and an emissivity value of 0.97 for water (Anderson, 1954),

$$H_{el} = 0.97\sigma (T_w + 273.15)^4, (4)$$

where σ is the Stefan-Boltzmann constant (5.67 × 10⁻⁸ W·m⁻²·K⁻⁴) and T_w is in degrees Celsius.

Latent heat H_l contributed by evaporation or condensation at the air-water interface can be expressed by the following equation (Hebert et al., 2011),

$$H_{lh} = (A + BU_w) (e_a - e_s), \tag{5}$$

where A and B are empirical constants derived from rigorous field measurements, U_w is the wind speed (m/s) at the water surface, e_s is the saturated vapor pressure (mm Hg) at the water surface, and e_a is the atmospheric water vapor pressure (mm Hg), which can be computed from the water temperature T_w and air temperature (T_a ; Troxler & Thackston, 1977; Fritz et al., 1980),

$$e_s = 25.37e^{17.62 - 5271/(T_w + 273.15)}, (6)$$

$$e_a = 25.37e^{17.62 - 5271/(T_a + 273.15)}r. (7)$$

Here, *r* is the relative humidity.

The surface convective heat flux H_c is the rate of sensible addition or removal of heat from the water to the overlying atmosphere. To find H_c , we use the function given by Hebert et al. (2011),

$$H_c = (3.66 + 1.83U_w) (T_a - T_w)P/1,000,$$
 (8)

which is based on the Bowen ratio (the ratio of sensible to latent heat flux; Bowen, 1926); P is atmospheric pressure (mm Hg).

The heat flux between river water and the riverbed is potentially a significant control on water temperature T_w , especially in shallow rivers, and perhaps even more so in rivers in permafrost terrain. Riverbed heat flux H_b consists of the amount of solar radiation absorbed by the bed material and the thermal conduction into the riverbed (Webb & Zhang, 1997),

$$H_b = -(1-R)H_{is}(1-a)(1-b)e^{-fh} - k_s \Delta T_b, \tag{9}$$

where a and b are the fractions of radiation absorbed by water and riverbed, respectively; f is the attenuation coefficient; h is water depth (m); and ΔT_b is the temperature gradient at the riverbed

found from a simple one-dimensional heat diffusion model (implemented as a finite difference code). The heat conduction equation for the riverbed can be written as (Hondzo & Stefan, 1994)

$$k_s \frac{\partial^2 T_s(z,t)}{\partial z^2} = \rho_s c_s \frac{\delta T_s(z,t)}{\delta t},\tag{10}$$

where $T_s(z,t)$ is subsurface temperature beneath the riverbed; z and t indicate depth (m) and time (s), respectively; and k_s , ρ_s , and c_s are the thermal conductivity (W·m⁻¹·°C⁻¹), density (kg/m³), and heat capacity (J·kg⁻¹·°C⁻¹) of the floodplain and channel bed deposits, respectively. The subsurface layer is bounded by a pair of parallel planes where z = 0 indicates the ground or channelbed surface and z = L indicates the depth of zero annual amplitude at which point the permafrost temperature T_c is constant year around,

$$T_s(0,t) = T_w, (11)$$

$$T_s(L,t) = T_c, (12)$$

$$\left. \frac{\partial T_s(z,t)}{\partial t} \right|_{z=L} = 0. \tag{13}$$

Generally, the water temperature T_w variability along a river is small compared to its temporal changes (Hebert et al., 2011). A one-dimensional model for a well-mixed river with vertically homogeneous T_w , as we assume is justified for shallow rivers on the Alaska North Slope, can be expressed by

$$\frac{dT_w}{dt} = \frac{\Delta H_w}{hc_w \rho_w},\tag{14}$$

where c_w and ρ_w are heat capacity (J·kg⁻¹·°C⁻¹) and density (kg/m³) of the river water, respectively. The initial water temperature is assumed to be 0 °C considering the mixture of ice and water directly after the river breakup. The river temperature model code is available in the permafrost modeling toolbox in both Matlab and Python versions (Overeem et al., 2018; https://github.com/permamodel).

2.2. Control Volume Permafrost Model

To investigate the permafrost thermal state of seasonally flooded river and delta floodplains, we need to propagate the simulated water temperature T_w as the upper boundary condition into a model that predicts permafrost temperature with depth (CVPM). CVPM is a nonlinear heat-transfer model for permafrost terrain recently developed by Clow (2018a). The model assumes advective heat flux is negligible compared to the diffusive heat flux, so that the enthalpy flux becomes a function of bulk thermal conductivity and temperature gradient. Unfrozen water contents below 0 °C are found taking in account interfacial, grainboundary, curvature, pore-water solute, and pressure effects. The model domain is highly flexible and can be set for a variety of dimensions, temporal and spatial scales. CVPM's numerical implementation is based on the control-volume method; namely, the model domain can be divided into discrete control volumes over which a given substrate is relatively uniform. Soil temperature T_s is computed at points located in the center of the control volumes, while the heat fluxes are computed at control-volume interfaces. CVPM is designed to account for a large variety of materials including deposits typical of river floodplains, such as organic rich materials, fine-grained sedimentary materials, sand, and gravel. Input variables required for CVPM include the initial conditions, boundary conditions (temperature or heat flux), and a number of parameters specifying the thermophysical properties of the soils or sedimentary materials (Table 1, No. 32-45). Output variables include soil temperature T_s, thermal diffusivity, volume fraction of ice, and liquid water content. For a detailed description of the physical basis of the CVPM model, we refer to Clow (2018a). The model code and user's manual (Clow, 2018b) are available at GitHub (https://github.com/csdms-contrib/CVPM/tree/v1.1).

All simulations for this study are one dimensional (vertical), even for the applications across the channelbelt and floodplain, as CVPM does not currently allow an undulating topographically variable upper boundary in two-dimensional implementations. Measured ground surface temperature $T_{\rm g}$, or water temperature $T_{\rm w}$ when either the channel contains water or the floodplain is inundated, serves as the upper boundary condition for the permafrost model. Then, subsurface thermal simulations are conducted to a depth of 70 m while the lower boundary heat flux is set to zero. The depth resolution of the model grid is 0.01 m for the upper 9 m and 6 m below that. It is an intractable problem to estimate a realistic initial condition in the absence of



continuous deep soil temperature measurements. One common strategy, which we employ as well, as an alternative for direct observations is to establish an equilibration profile with long-term ground temperature records (Riseborough et al., 2008). In this study, an initial subsurface temperature profile is established by a 100-year spin-up procedure with repeated annual ground surface temperature T_g cycles.

3. Model Validation and Application, Kuparuk River Delta

3.1. Site Description

Climate and hydrological measurements are limited in the Arctic region. The Kuparuk fluvio-deltaic plain located on the North Slope of Alaska is selected to validate the combined model and conduct simulations because it has been relatively well researched and has a long-term record of hydrologic measurements. The Kuparuk River flows northward across the Arctic Coastal Plain to the Beaufort Sea (Figure 2). The watershed (8,421 km²) is underlain by continuous permafrost (Lachenbruch & Marshall, 1986) and has a maximum elevation of 263 m (Déry et al., 2005). Permafrost thickness ranges from less than 200 m near the foothills to over 600 m near the coast in the Prudhoe Bay area (Lachenbruch et al., 1988). The coastal plain is dominated by ice-wedge polygons, thermokarst lakes, and sedge tundra (Taras et al., 2002). Snowfall accounts for about 50% of the annual precipitation and may occur at any time of the year in the Kuparuk River Basin (Déry et al., 2005). River flow in the headwaters typically begins in late May while the freshet arrives at the coast by early June. Freezeup season typically begins in mid-September, but some water may flow until October (McNamara et al., 1998). Daily river discharge Q has been measured at the U.S. Geological Survey (USGS) hydrologic station 15896000 (70°16′54″N, 148°57′35″W) since May 1971. River temperature T_w has been measured discontinuously at the same site. Hydrological data for this study were obtained at the USGS Water Data website (https://waterdata.usgs.gov/nwis/uv?15896000). No air temperature T_a or soil temperature T_s measurements are available in the Kuparuk River or its delta. Fortunately, daily T_a and T_s have been recorded at a nearby combined meteorological and permafrost monitoring station (Deadhorse, 70°09'42.4"N, 148°27'49.6"W) since 2001. The Deadhorse station located near Prudhoe Bay is maintained by the Geophysical Institute of the University of Alaska Fairbanks and is about 20 km away from the USGS hydrologic station.

We use temperature measurements from the Deadhorse station over 8 years (2001–2008) and establish an average temperature regime for that period, which is then repeated for 100 years to spin up the CVPM model and arrive at a representative initial temperature profile for our subsequent simulations. Our subsequent experiments are driven by climate data over the period 2009–2017.

Mean-annual air temperature T_a and ground surface temperature T_g at the Deadhorse station over 2009–2017 were -9.96 °C and -2.83 °C, respectively. Generally, T_a and T_g are close from May to September, while T_g is about 11 °C higher than T_a from October to April due to the insulating effect of the seasonal snow cover (Zhang, 2005; Figure 3a). The watershed is covered with snow for 7–9 months (McNamara et al., 1998). River runoff peaks are associated with spring snowmelt, with secondary contributions due to summer rainfall (Déry et al., 2005). Snowmelt occurring between mid-May and mid-June is the most significant hydrologic event of the year and provides about 70% of the river's annual runoff into the Arctic Ocean (McNamara et al., 1998).

River stage S is a crucial parameter in the water temperature T_w simulations; however, it is not provided directly by the USGS data repository. Upon request, research hydrologists at the USGS in Anchorage provided the stage-discharge rating curve for the USGS hydrologic station. From this curve, the river stage can be back-calculated as (Figure 3b)

$$S = G - G_0 = 1.173 \ln(Q + 253.3) - 6.2, \tag{15}$$

where G is gauge height (m); G_0 stands for the gauge height offset (8.02 m; Figure 3b).

3.2. Model Validation

Water temperature T_w simulated by the river-water thermal model is validated against observations over the 2014–2016 time period. Sources for the input variables are listed in Table 2. Air temperature T_a and discharge Q records are obtained from the University of Alaska Fairbanks Deadhorse permafrost-monitoring

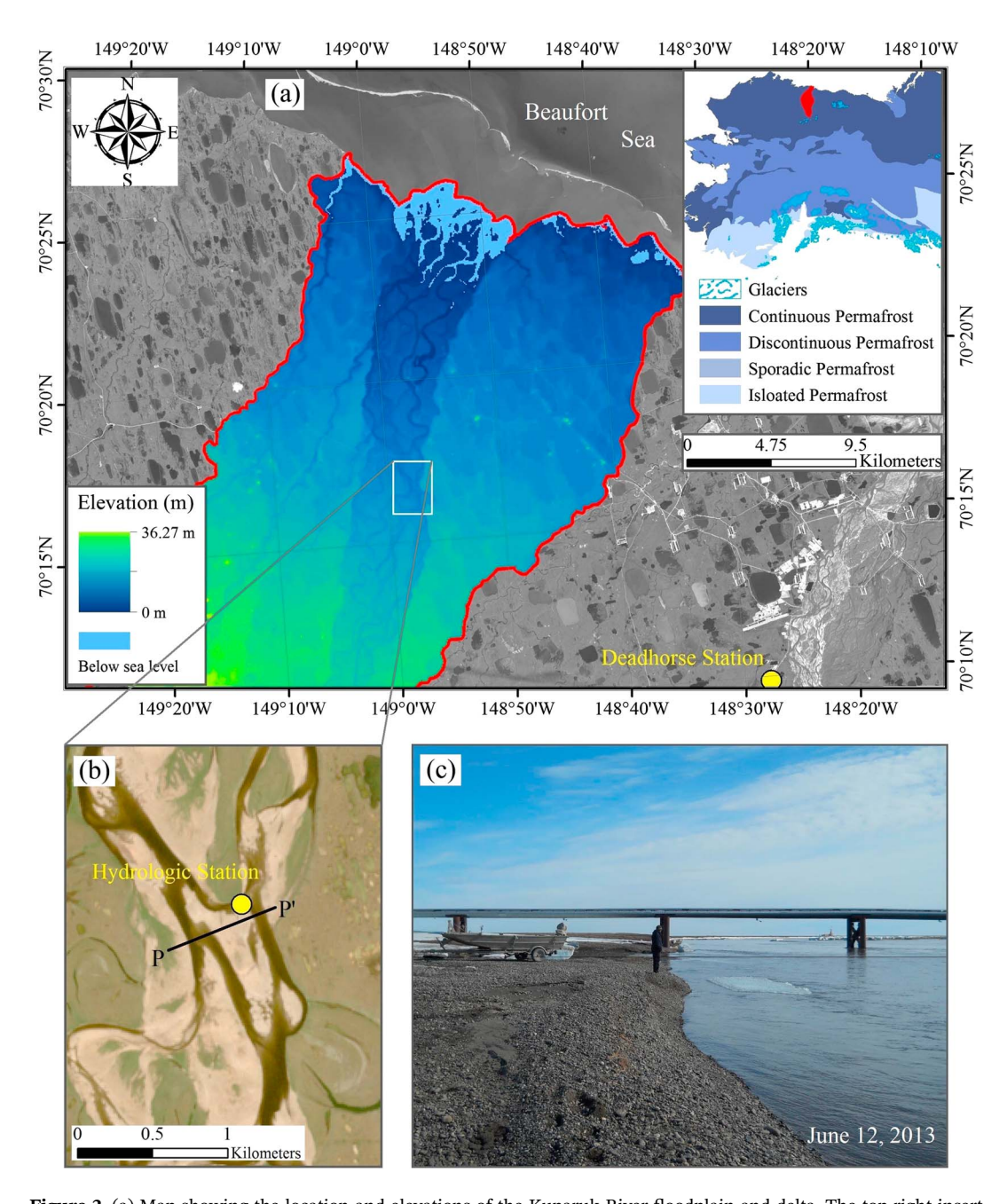


Figure 2. (a) Map showing the location and elevations of the Kuparuk River floodplain and delta. The top right insert shows permafrost distribution in Alaska and the location of the Kuparuk River watershed (red area). Surface elevations are from the ArcticDEM (Porter et al., 2018; https://www.pgc.umn.edu/data/arcticdem/). (b) Location of the U.S. Geological Survey (USGS) hydrologic station 15896000 and the river cross-section P-P' used in sections 3.4 and 4.3 (black line). The base map is a Sentinel-2 image acquired on 29 July 2017, obtained from the Copernicus Open Access Hub (https://scihub.copernicus.eu/). (c) Photograph showing the Kuparuk River and the adjacent floodplain at the USGS hydrologic station (photograph taken by Jason Baker, USGS Fairbanks field office, 12 June 2013).

station and the USGS Kuparuk hydrologic station, respectively. Other meteorological parameters are obtained from the ERA-Interim reanalysis (79-km grid spacing) provided by the European Centre for Medium-Range Weather Forecasts (Dee et al., 2011), which is the currently recommended data set for the Alaskan North Slope (Lader et al., 2016). Water surface albedo R is set to 0.2, as is found to be typical for shallow water gravel bed and turbulent rivers in British Columbia, Canada (McMahon & Moore, 2017). Deposits in the Kuparuk floodplain are predominately sand and gravel (Shiklomanov & Nelson, 1999).

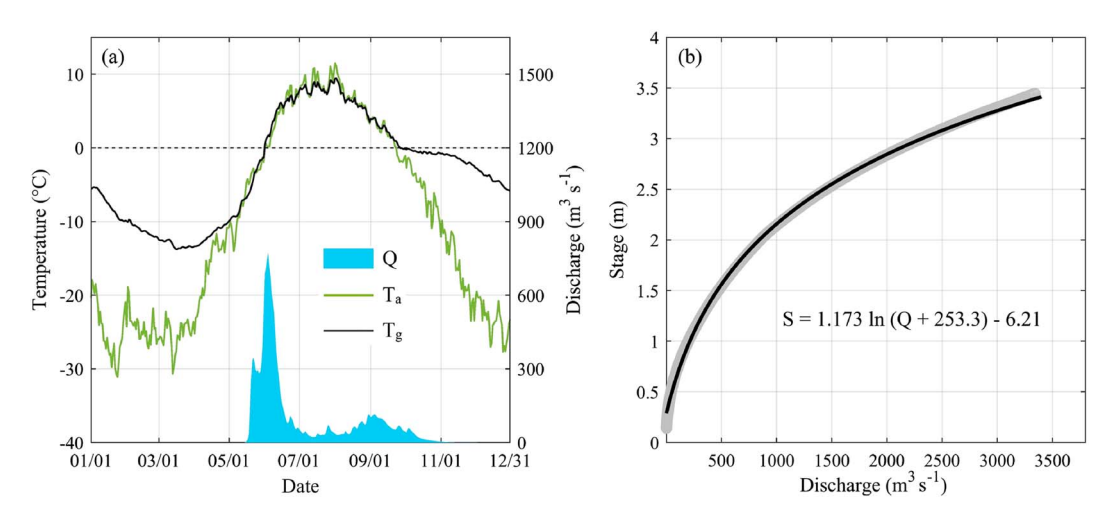


Figure 3. In situ measurements in the Kuparuk River during 2009–2017. (a) Mean-daily air temperature T_a (green line), ground surface temperature T_g (black line), and river discharge Q (blue bars) over 2009–2017. (b) Gray dots show Q versus stage S; black line indicates the logarithmic regression to the discharge data.

Morphologically, the Kuparuk River is considered to be similar to the Canadian rivers. Soil depth of zero annual amplitude L is the depth at which soil temperature T_s is constant (T_c) and is thus unaffected by seasonal ground surface temperature T_g variations. Since no in situ soil temperature records are available in the riverbed, T_c is assumed to be -5 °C at \sim 30 m as determined from sensitivity tests run with CVPM forced by the daily mean T_g over 2009–2017.

Onset and end date of water occurrence are determined by the first and last day with discharge Q > 1 m³/s. Accordingly, river flow and inundation lasted from mid-May to mid-November during 2014. River stage S is retrieved from Q based on equation (15) (Figure 4a). With the input variables listed in Table 2, we calculate the heat flux components (Figure 4b) and T_w (Figure 4c). Net solar radiation H_{sr} was the dominant control on the heat balance before October. Over this period, the negative riverbed heat flux H_b indicates heat penetrates into the subsurface and warms the riverbed. Air temperature T_a was below freezing point after October accompanied by the decreasing H_{sr} . Meanwhile, the waterbody lost heat mainly through longwave emission and surface convection (Figure 4b). Simulated water temperatures T_w agreed well with the in situ measurements. Water temperatures increased gradually in late May even when T_a was below the freezing

Variable	Source						
Surface air temperature (T_a)	Deadhorse station						
Discharge (Q)	Kuparuk hydrologic station						
Incoming solar radiation (H_{is})	3-hourly ERA-Interim						
Downward longwave radiation (H_{dl})	3-hourly ERA-Interim						
Wind speed (U_w)	3-hourly ERA-Interim						
Atmospheric pressure (P)	3-hourly ERA-Interim						
Relative humidity (<i>r</i>)	6-hourly ERA-Interim						
Aerated water surface albedo (R)	0.2 (McMahon & Moore, 2017)						
Empirical constants for H_l calculation (A, B)	A=6, B=3 (Hebert et al., 2011)						
Fraction of radiation absorbed in water (a)	0.6 (Webb & Zhang, 1997)						
Fraction of radiation absorbed in riverbed (b)	0.2 (Webb & Zhang, 1997)						
Attenuation coefficient (f)	0.05 (Webb & Zhang, 1997)						
Depth of zero annual amplitude (L)	30 m (Simulated by CVPM)						
Temperature at $L(T_c)$	−5 °C (Simulated by CVPM)						
Heat capacity of water (c_w)	4,210 J kg ⁻¹ K ⁻¹ (Jarosch & Gudmundsson, 2012						
Density of water (ρ_w)	1,000 kg/m ³ (Jarosch & Gudmundsson, 2012)						

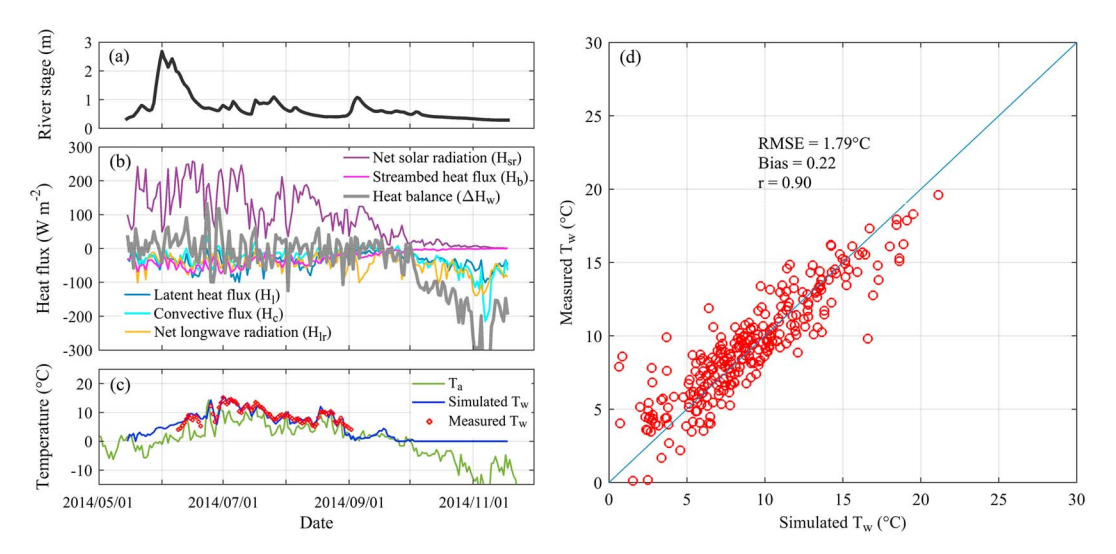


Figure 4. Simulations and validations of water temperature T_w in the downstream Kuparuk River. (a) River stage S derived from discharge Q in 2014; (b) simulated heat flux components in 2014; (c) measured air temperature T_a , T_w and simulated T_w in 2014; (d) scatter diagram shows the simulated T_w versus measured T_w over 2014–2016. RMSE = root mean square error.

point. Most of the time (88% of the cases), T_w of streamflow was higher than T_a . Water temperatures remained ~0 °C when T_a fell below the freezing point after October (Figure 4c). We compare the simulated T_w with measured T_w in the downstream Kuparuk River during 2014–2016 in Figure 4d. The root mean square error, bias, and correlation coefficient between the T_w simulations and measurements were 1.79 °C, 0.22 °C, and 0.90, respectively.

In order to test CVPM's performance in a permafrost temperature T_s simulation, we validate the CVPM model against T_s observations at the nearby Deadhorse station. Sedimentary materials near Prudhoe Bay include peat, silt, sand, and gravel (Zhang et al., 1996). Physical and thermal properties of these materials are set based on descriptions from the literature (Benscoter et al., 2011; Clow, 2018b; Lachenbruch et al., 1982; Shiklomanov & Nelson, 1999) and are summarized in Table 3.

The validations are conducted for 2014–2015 when temperature sensors at the Deadhorse station are known to have been unaffected by frost heave and thus remained at fixed depths. Soil temperatures at a range of depths simulated by CVPM are compared with the corresponding measured T_s values during 2015 in Figure 5. Simulated ground temperatures T_s generally agree well with measured T_s , especially for the upper layers. During winter, simulated T_s is systematically higher than observed T_s at and below depths of 18 cm. Temperature biases primarily exist during freeze/thaw transitions in the deeper layers (Figure 5a). During the freezing period, measured T_s kept nearly constant at the freezing point due to the release of large quantities of latent heat (i.e., the zero curtain effect), especially in the deeper layers. However, the simulated T_s does not appear to describe this effect. This is also evident in the scatter diagrams shown in Figure 5b. Root mean square error, bias, and correlation coefficient between the simulated and observed soil temperatures for all depths were 1.17 °C, -0.22 °C, and 0.98 during 2014–2015. These validation experiments demonstrate that with the selected thermophysical parameters (Table 3), CVPM generally matches permafrost temperatures well in the active layer and the shallow soil profile.

Table 3 Physical and Thermal Properties of Sedimentary Materials															
Depth	Soil type	k_s	$\rho_{\rm s}$	c_s	S_0	h_s	Φ_0	$\Phi_{\rm c}$	h _c	S_{r}	$\chi_{_{S}}^{*}$	λ	d_1	d_2	n_2/n_1
0-0.2 m	Peat	0.25	330	1,920	0.0	0	0.40	0.20	2.0	1	0.003	0.33	4	0.1	6.0
0.2-2 m	Silt	2.10	1400	730	1.5	10	0.40	0.05	2.0	1	0.003	0.39	10	2.0	2.6
2-70 m	Sand and gravel	2.30	1250	660	0.8	10	0.45	0.15	3.0	1	0.003	0.36	180	30.0	0.0

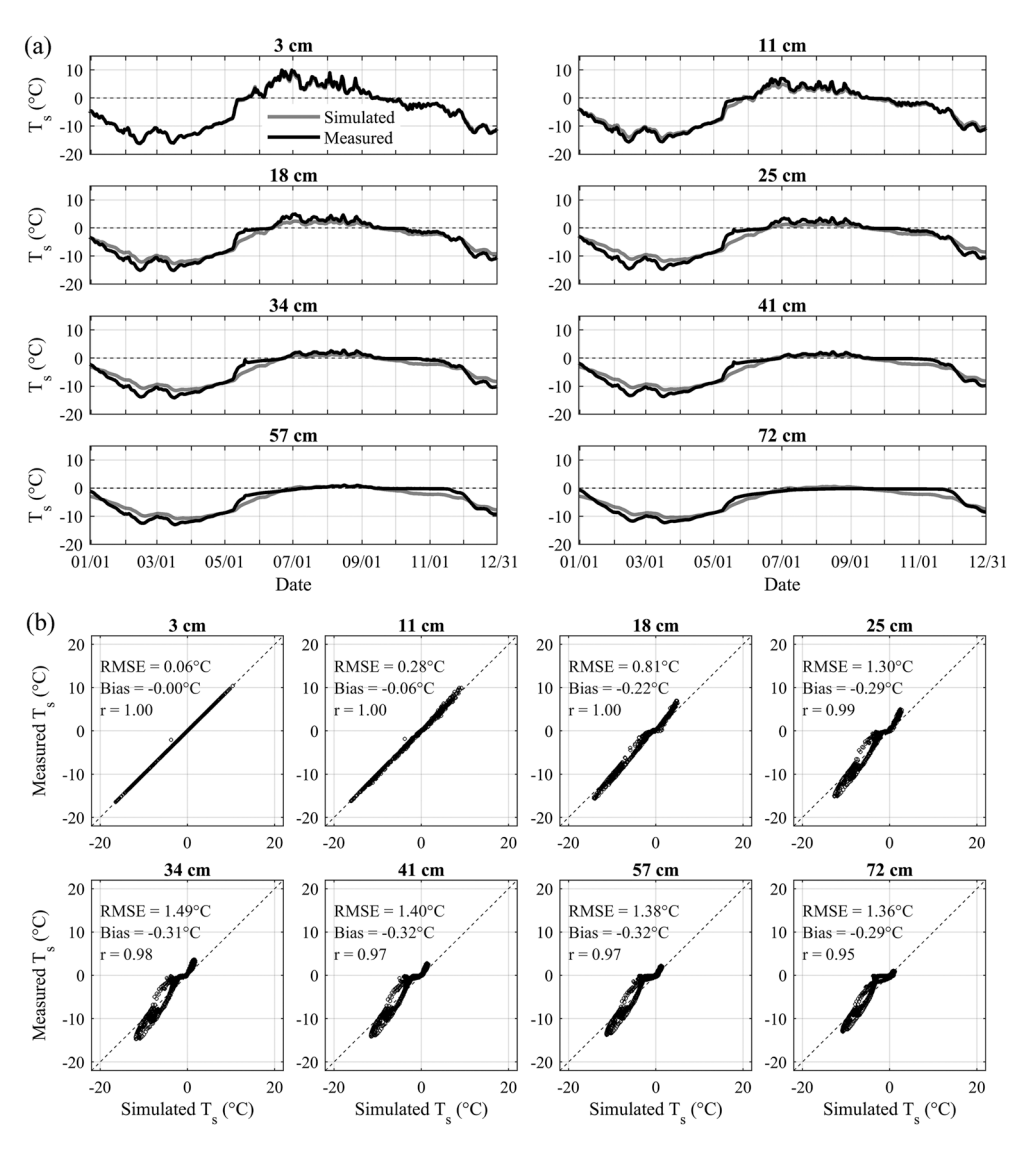


Figure 5. Validation of soil temperature T_S simulated by control volume permafrost model at the University of Alaska Fairbanks Deadhorse station. (a) Comparisons between simulated T_S (light gray lines) and measured T_S (black) at different depths in 2015; (b) scatter diagram shows the simulated T_S versus measured T_S over 2014–2015. RMSE = root mean square error.

3.3. Permafrost Temperature Beneath the Riverbed

Here, we investigate the permafrost thermal regime beneath the sand- and gravel-dominated riverbed in the downstream Kuparuk River based on the coupling of our river water temperature model and CVPM. First, we simulate water temperature T_w between 2009 and 2017 (Figure 6a). On average, T_w of streamflow (5.79 °C) was more than 2 °C higher than the dry land ground surface temperature T_g (3.49 °C) found at the Deadhorse station over the same period. The CVPM model is initialized by the 100-year spin-up based on the repeated mean-daily ground surface temperature T_g over 2001–2008; then we simulate the subsurface soil temperature T_s of the riverbed forced by the combination of measured T_g and simulated T_w (if the riverbed is inundated) during 2009–2017. A controlled experiment without any channel flow or inundation is conducted over the same period (Figure 6b). Our experiments demonstrate that river inundation significantly warmed the underlying permafrost, resulting in a deepening of the thaw front (Figure 6c). Over the flow and flood seasons, sustained riverbed warming can be detected at depth, and this warming lasted until the next year, especially for 2014–2017. Soil temperatures beneath the inundated riverbed can be 1 °C higher even at a depth of 8 m (Figure 6d).

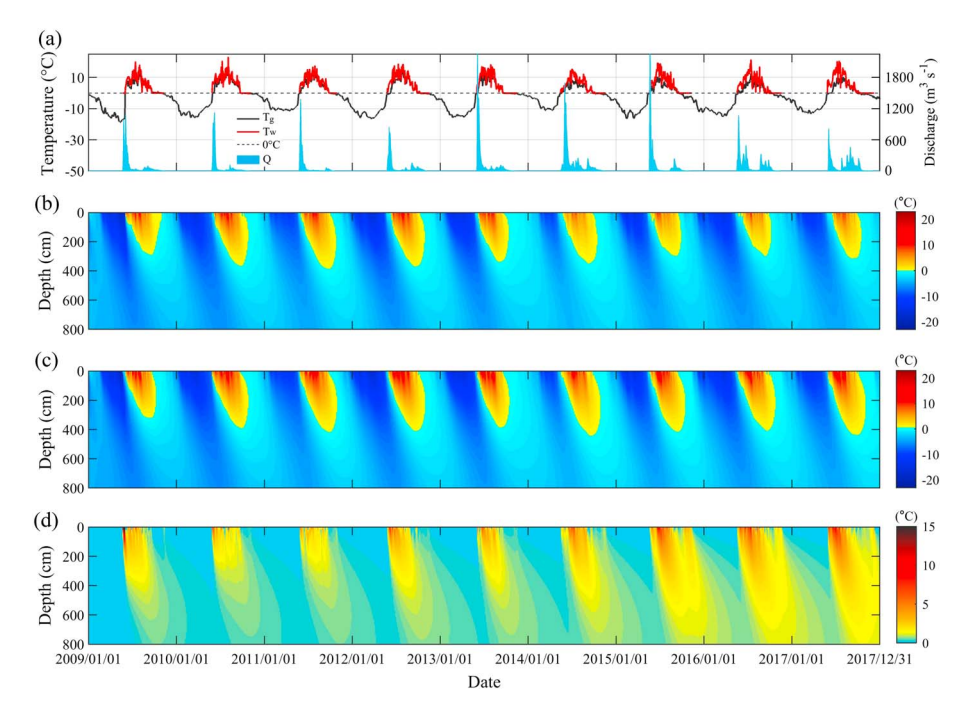


Figure 6. Riverbed permafrost thermal state simulated for 2009–2017. (a) Measured ground surface temperature T_g , simulated water temperature T_w , and river discharge Q; (b) simulated riverbed soil temperature T_s without inundation; (c) simulated T_s with inundation; (d) T_s with inundation minus T_s without inundation.

Over the period 2009–2017, the Kuparuk River flow and inundation onset date varied from mid-May to early June, and the runoff end date varied from late October to late November (Figure 7a). On average, the mean-annual ground surface temperature T_g under conditions of inundation was about 1 °C higher than that simulated for the controlled experiment without any inundation (Figure 7b). As a result, the active layer deepened with the presence of standing water, ranging from 67 cm in 2010 to 183 cm in 2017 with an average value of 118 cm (Figure 7c). The riverbed warmed by more than 1 °C on average during 2014–2016 when river inundation onset was much earlier than in previous years. ALT with streamflow was more than 150 cm deeper than that without standing water. The mean-annual T_g was highest in 2014, associated with the earliest flow and inundation onset. For these conditions, the corresponding ALT with inundation reached the maximum (504 cm).

3.4. Permafrost Thermal State for a River and Floodplain Cross Section

Permafrost temperatures and ALT across the Kuparuk floodplain are simulated during 2009–2017, a period during which the inundation timing and extent differ significantly in high- and low-flow years (the reader can find the analysis of river dynamics in section 4.1). Here, we investigate the permafrost thermal state for a river cross section close to the USGS hydrologic station 15896000 (P-P' shown in Figure 2). The river cross section includes two main river channels and the floodplain in between. Based on the 2-m high-resolution ArcticDEM (Figure 8a), inundation along the profile during 2009–2017 occurs when the floodplain is submerged according to the river stage. We assume the water temperature T_w is homogeneous along the river cross section. A combination of measured ground surface temperature T_g and simulated T_w (if a specific location is inundated) is used to simulate the permafrost temperature T_s across the profile.

As expected, the low-lying river stream channels had long flow durations. In contrast, the intermediate and outer floodplains were submerged only during the spring snowmelt flood, and then mostly in high-flow years (e.g., 2014; Figure 8b). Streamflow seldom reached the outer floodplain in relatively low-flow years (2010–2012). Compared with the outer floodplain, the river channels had much higher permafrost temperatures during the flood season (see Animation S1 in the supporting information). Mean-annual ground temperature (MAGT) increased from the channel edges to the middle of the river (Figure 8c). As a consequence, the active layer beneath the riverbed reached more than 500 cm in 2014 when river discharge reached a maximum, which was about 120 cm deeper than in locations without river inundation (280 cm). Increase of ALT

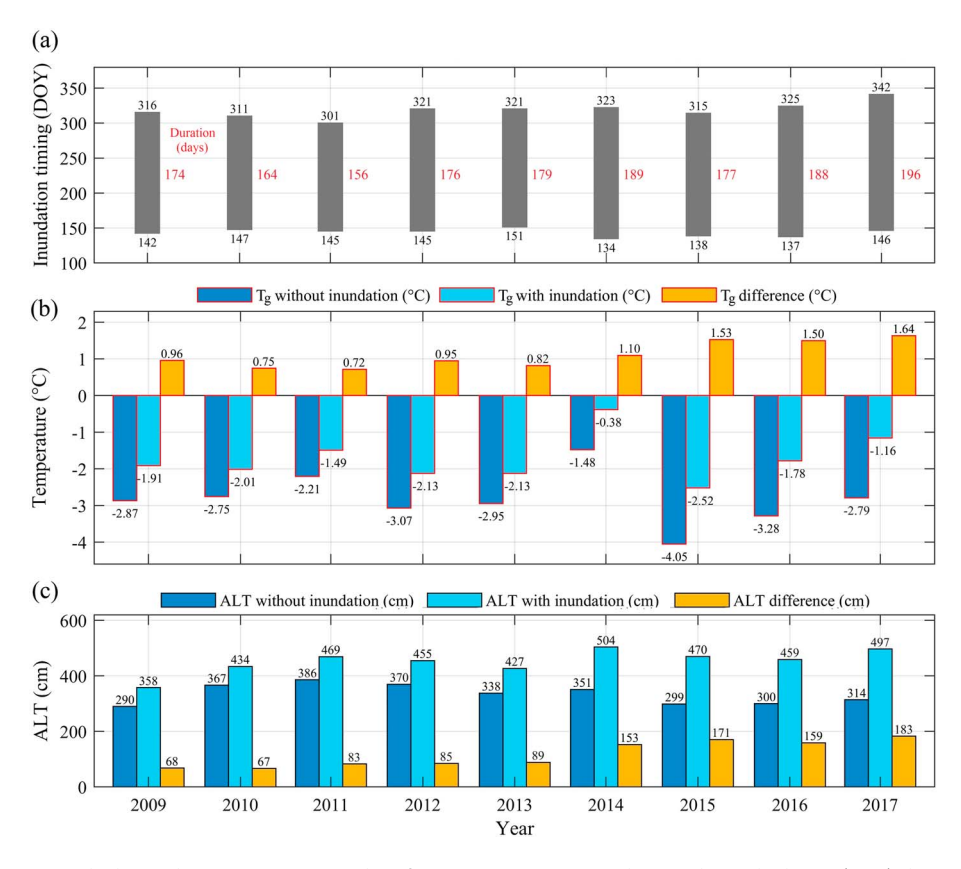


Figure 7. Riverbed inundation timing, ground surface temperature T_g , and active layer thickness (ALT) during 2009–2017. (a) Inundation timing: DOY refers to the day of year, and numbers in red indicate the inundation duration; (b) mean-annual input T_g with and without inundation, as well as their difference; (c) ALT with and without inundation, as well as their difference.

in the floodplain during the ephemeral spring flood can reach about 30 cm compared with the dry land. Thus, river inundation plays an important role in ALT variations over the floodplain. ALT difference between the river channel and floodplain reached more than 150 cm in 2014, whereas their difference was considerably smaller in low-flow years (e.g., about 70 cm in 2011; Figure 8d).

3.5. Sedimentary Characteristics as a Control on Permafrost's Response to Inundation

Effects of streamflow on permafrost vary with different sedimentary characteristics and associated bulk properties of the subsurface. Deposits vary considerably across different Alaskan Arctic river floodplains and vary along each river's longitudinal profile. The floodplain in the Kuparuk River Delta is underlain by marine deposits, while the floodplain of the Hulahula and Jago Rivers (eastern Arctic Coastal Plain) is dominated by coarse alluvial fan deposits (Karlstrom, 1964). Our simulations assume homogeneous sand and gravel in the floodplain. However, we realize the floodplain deposits are variable, and generally, the grain size of floodplain deposits decreases from the main channel to the edge of the floodplain. While sand and gravel dominate the deposits in the downstream Kuparuk River (Shiklomanov & Nelson, 1999), river channels in more silty and organic rich layers have also been widely found in the Kuparuk watershed (Brosten et al., 2006). In addition, higher parts of the floodplain often are covered in peats and moss and form an organic-rich layer on top of the sedimentary material.

We investigate the permafrost thermal state in the floodplain with sedimentary material set as end-members of homogeneous sand and gravel, or sand and gravel deposits capped with a peat layer in the upper 30 cm (Figure 9). Model parameters for deposits are the same as listed in Table 3. In either case, the riverbed subsurface is significantly warmed, and thaw bulb expands under river inundation. Sand and gravel profiles without peat respond much more quickly to thermal input and river inundation. With streamflow the ALT in sand and gravel riverbed increases from 307 to 408 cm. In contrast, when a 30-cm peat and

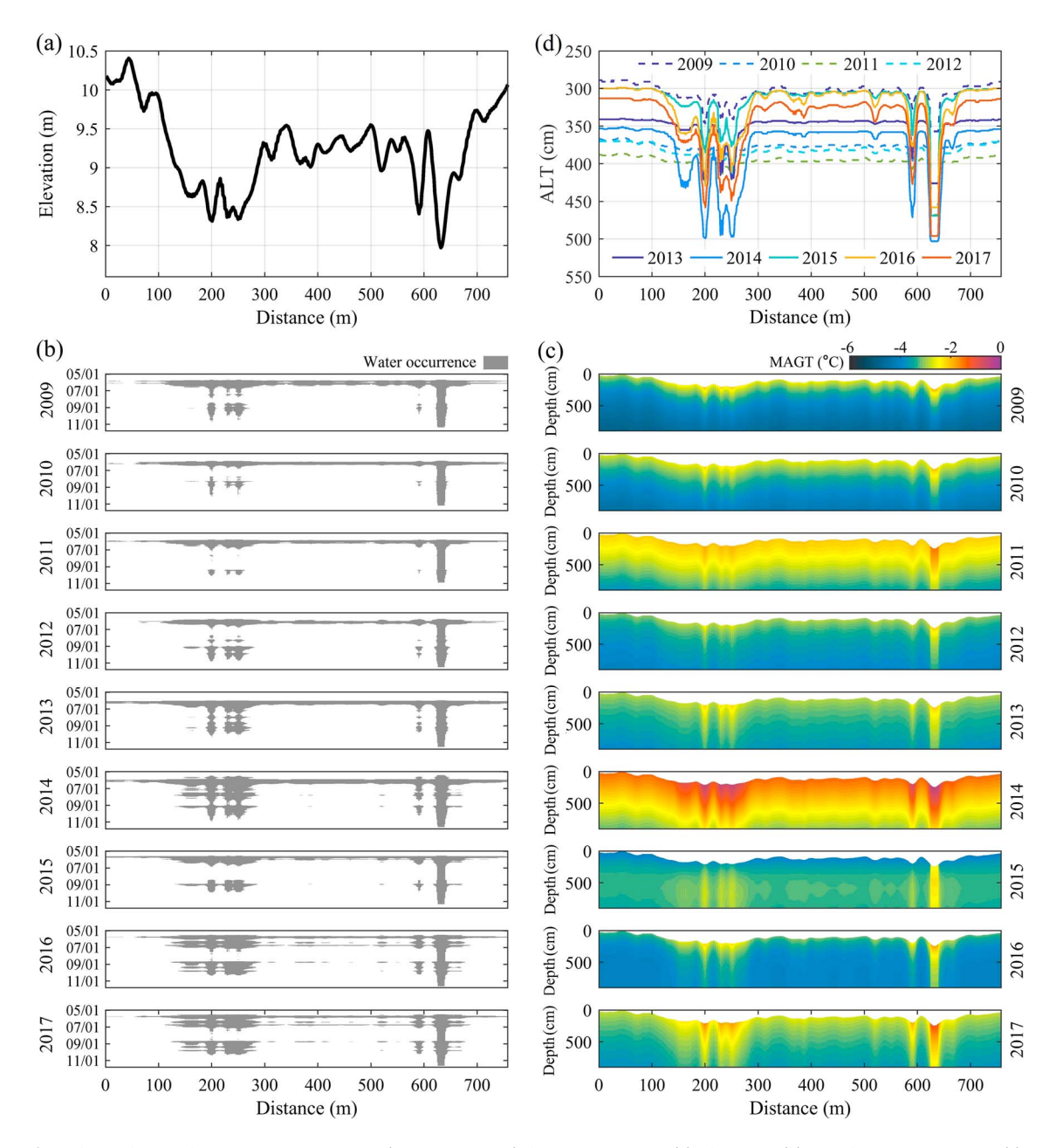


Figure 8. Permafrost thermal state along a river cross section (P-P' in Figure 2) during 2009–2017. (a) Elevation; (b) inundation occurrences; (c) simulated mean-annual ground temperature (MAGT); (d) simulated active layer thickness (ALT).

organic matter-rich top layer is assumed to be present, the ALT of dry land is only 64 cm, which is close to the general ALT estimations in Kuparuk River Basin (Nelson et al., 1997). Under inundation, the active layer underlying such a peat-capped profile increases to 133 cm. Due to the higher thermal conductivity, permafrost underlying the coarse-grained deposits is more sensitive to river inundation, whereas peat layers in floodplains provide an insulating effect due to its lower thermal conductivity. The ALT of a sand and gravel riverbed decreases by 21% with a 30-cm top peat layer in the noninundated case and by 33% in the inundated case.

4. Effect of River Dynamics on Permafrost Thermal State

As demonstrated in sections 3.3 and 3.4, inundation occurrence plays an important role in permafrost thermal state. We further investigate the effect of river dynamics on permafrost temperature and ALT in this

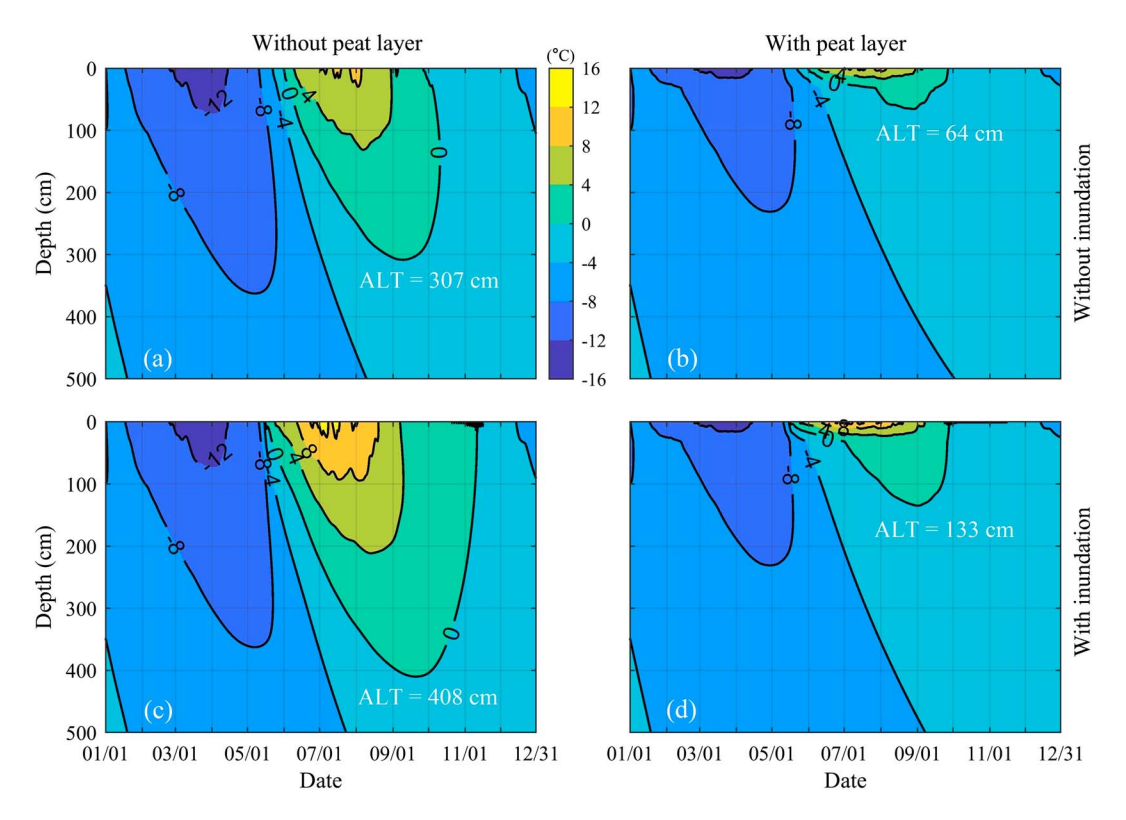


Figure 9. Riverbed and floodplain permafrost temperature T_S for different sedimentary profiles. (a) Sand and gravel riverbed without inundation; (b) organic-capped floodplain without inundation; (c) sand and gravel riverbed with inundation; (d) organic-capped floodplain with inundation. ALT = active layer thickness.

section. First, we examine the observed changes of inundation timing and river discharge in the downstream Kuparuk River over the past four decades. Based on this analysis, sensitivity experiments are conducted to investigate the response of permafrost to varying inundation timing and discharge.

4.1. Kuparuk River dynamics

We examine the changes in inundation timing and discharge based on the hydrologic observations, as well as the Landsat-based (30-m spatial resolution) water bodies dynamics in the downstream stretch of the Kuparuk River (Figure 10 after Pekel et al., 2016). On average, river streamflow started on 25 May (day of year [DOY] 144±7) and ended on 7 November (DOY 310±14) during 1978-2017. No statistically significant trend in inundation onset during 1978-2017 is found due to the large variability, which is typical in Arctic river systems (Figure 10a). The runoff season ended later with a rate of 6.06 days per decade (99% confidence level; Figure 10b). Thus, inundation duration became longer at a rate of 6.45 days per decade (99% confidence level) (Figure 10c). On average, the mean-annual river discharge was 42±14 m³/s over the past four decades. Mean-annual river discharge showed a significant increase (95% confidence level) at a rate of 3.74 m³·s⁻¹·decade⁻¹ (+35% overall; Figure 10d). In Figure 9e, we present the inundation map for the lowermost stretch of the Kuparuk River and its delta. This data set was obtained from the Global Surface Water Explorer, which reports surface water dynamics over 1984-2015 based on Landsat imagery (we refer to Pekel et al., 2016, for a detailed description of the global data set). It is evident from the transition map that surface water bodies in Kuparuk River Delta have experienced vast changes. Notably, new permanent water and seasonal water emerged along the river channels between 1984 and 2015 (with the caveat that in Arctic Alaska, good quality, cloud-free coverage for this data set does not always span the whole time period of 1984-2015).

4.2. Effect of Inundation Timing on Permafrost Thermal State

Considering the large variations in river inundation presented in Figure 10, we simulate water temperature T_w and riverbed soil temperature T_s with varying inundation onset dates in the downstream Kuparuk River.

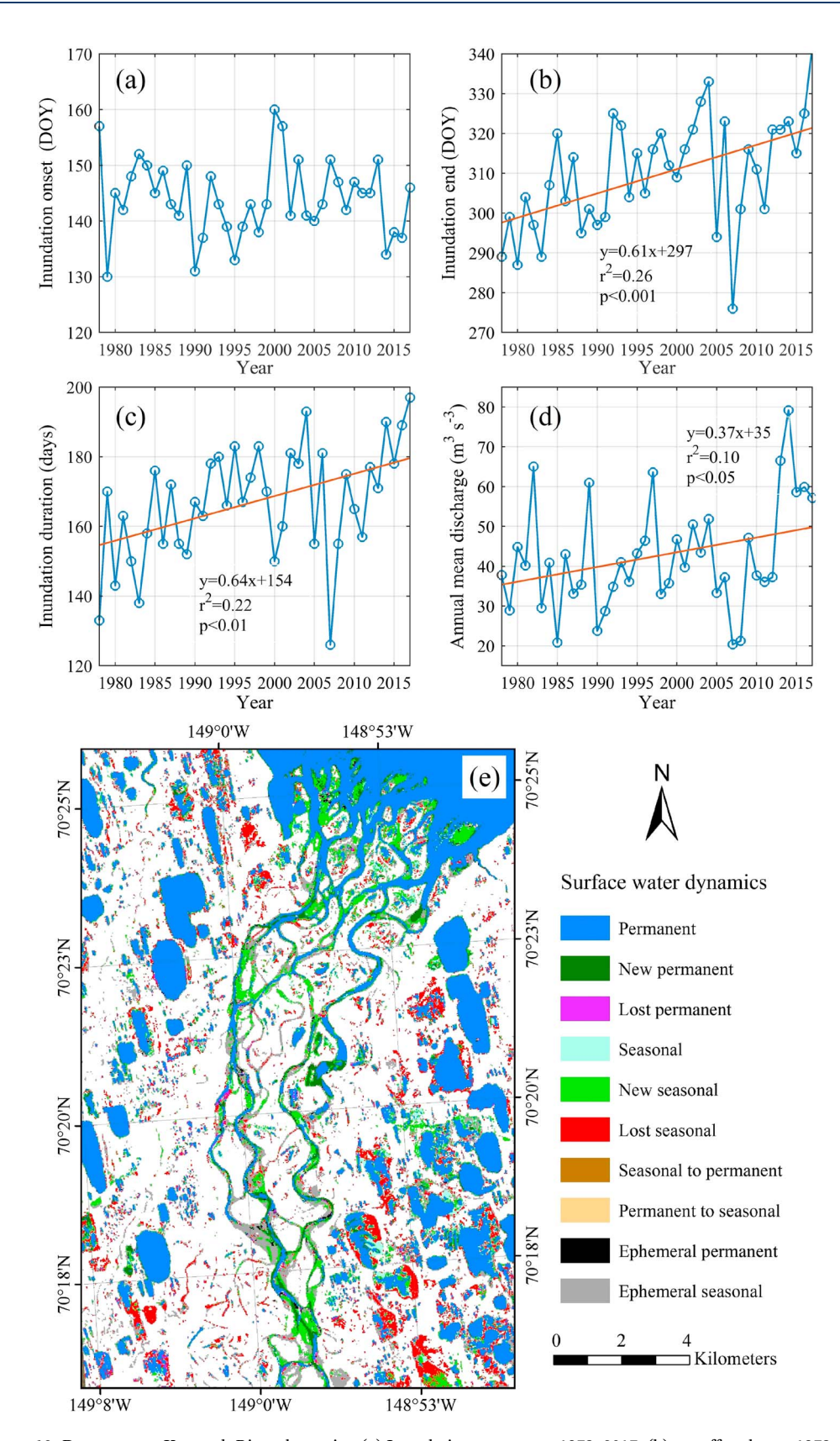


Figure 10. Downstream Kuparuk River dynamics. (a) Inundation onset over 1978–2017; (b) runoff end over 1978–2017; (c) inundation duration over 1978–2017; (d) mean-annual river discharge over 1978–2017; (e) surface water body dynamics in the Kuparuk River Delta during 1984–2015 (Pekel et al., 2016). DOY = day of year.

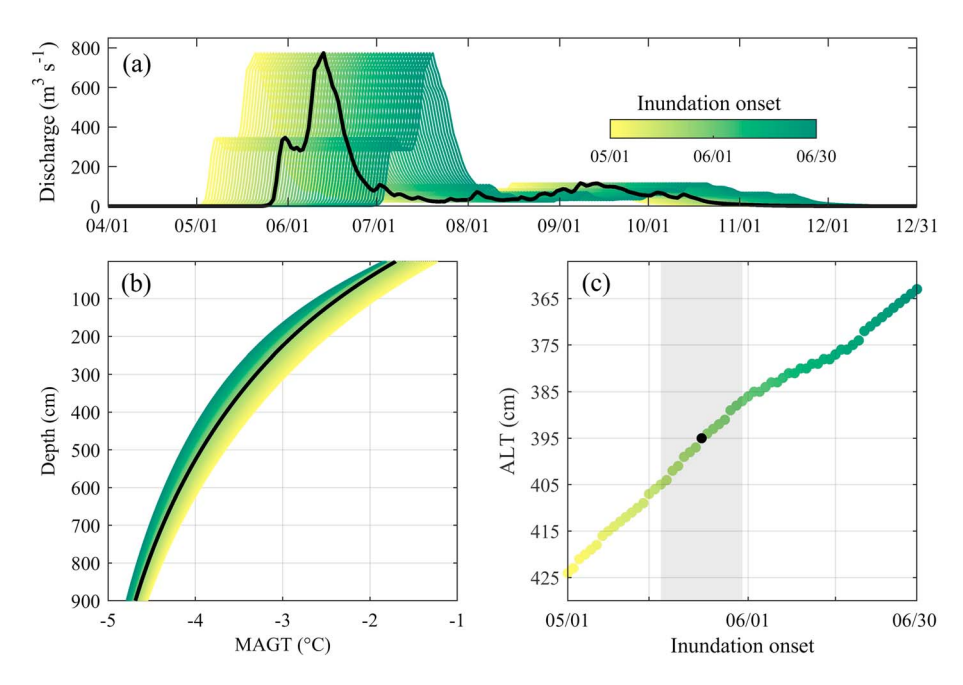


Figure 11. Effect of inundation onset on permafrost thermal state. (a) River discharge *Q* with inundation onset varying from 1 May to 30 June, while the inundation duration remains constant; (b) mean annual ground temperature (MAGT); (c) active layer thickness (ALT). Black lines and point represent river inundation beginning on day of year 144; gray shadow indicates inundation starts on DOY 144±7 (see Animation S2).

Simulations are driven by mean-daily air temperature T_a , ground surface temperature T_g , and discharge Q over 2009–2016 (Figure 3a). Other model parameters are set as listed in Table 2. While we assume a stable runoff duration, experiments are conducted with stepwise varying inundation onset (Figure 11a). Varying

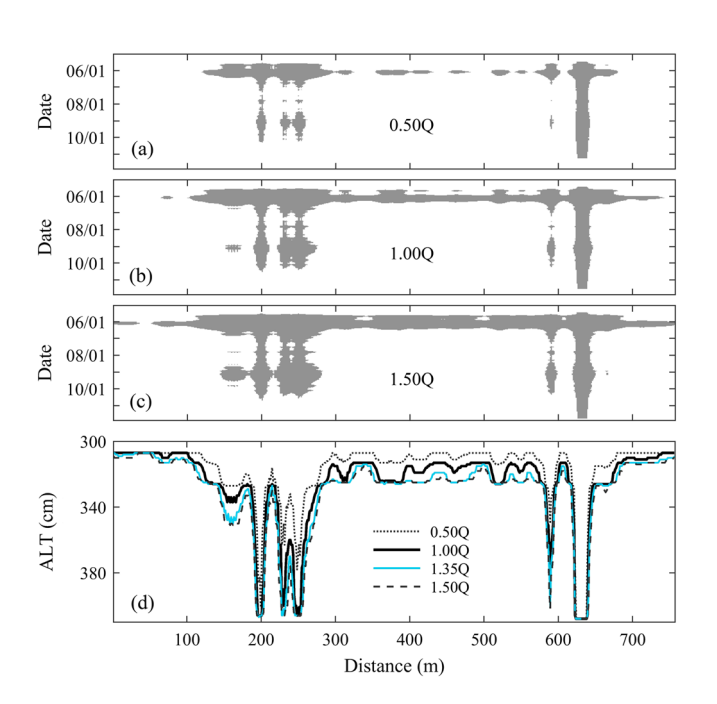


Figure 12. Inundation timing along the river cross-section P-P' with (a) discharge *Q* declining by 50% (0.5*Q*), (b) keeping the same (1.0*Q*), and (c) increasing by 50% (1.5*Q*); (d) active layer thickness (ALT) along the river cross section with different discharge scenarios.

the inundation onset from May 1 (DOY 121) to June 30 (DOY 181) results in significant MAGT variations (Figure 11b). In general, permafrost temperatures increase with the earlier arrival of inundation. Riverbed MAGT with inundation onset starting on DOY 121 can be more than 0.5°C higher than that starting on DOY 181. As a consequence, the riverbed ALT increases by more than 60 cm (Figure 11c). Flood water temperature T_w is much higher than the dry land T_g in the early snowmelt-controlled inundation season (Figure 6) and thus has sustained effect on riverbed permafrost temperature, while the effect of rainfall-runoff in late inundation season is relatively limited. This is because both the T_w and T_g remain constant around the freezing point in late runoff season (see in Figures 4 and 6). It takes time for heat to transfer into soils and warm the permafrost. These experiments suggest that the observed earlier arrival of river inundation in recent years would have resulted in the riverbed permafrost warming.

4.3. Effect of River Discharge on Permafrost Thermal State

Changes in river discharge can alter inundation timing, but in addition, we hypothesize that an increased stage affects flood water extent across the floodplain, with consequent effects on permafrost thermal state. We simulate permafrost temperatures T_s along profile P-P' for different discharge scenarios (Figure 12). Inundation timing across the profile changes significantly when the daily Q (black line in Figure 11a) declines by 50% (0.5Q) or alternatively increases by 50% (1.5Q). With a 50% decline in daily Q, the mean inundation duration across the profile decreases from 28 days to 15 days, and flood water only seldom reaches the floodplain edges. As a



consequence, mean ALT along the profile as a whole decreases by 8 cm within a single year. Even in the main river channels, the active layer can become about 40 cm shallower. In contrast, with a 50% increase in daily Q the mean inundation duration across the profile increases by 10 days. On average, the active layer along the profile deepens by 7 cm. Moreover, ALT in low-lying depressions or chute channels beside the main river channels can increase by more than 30 cm. The experiments also suggest that the observed 35% increase of mean annual discharge (1.35Q) in the downstream Kuparuk River observed since the 1970s would result in extensive deepening (up to about 10 cm) of the active layer over the floodplain within a single year. The increase in ALT may be more significant in reality as the observed increase in Q has occurred over four decades. Permafrost across the floodplain is vulnerable to such enhanced river discharge associated with the extension of water bodies and the prolonging of spring flood. The deepest channel always carries water during the runoff season, and changing river discharges have less effect on its underlying permafrost.

5. Discussion

5.1. Uncertainties

Our deterministic model of river-water temperature T_w has significant simplifications: Heat fluxes contributed by lateral inflow, precipitation, and fluid friction are not included. Whereas we consider this an important shortcoming, a recent study on Arctic river energy balance suggested lateral inflow heat flux has little influence on T_w (King et al., 2016). Also, most studies have neglected the heat flux contributed by precipitation in the modeling of river water temperature (e.g., Ahmadi-Nedushan et al., 2007; Toffolon & Piccolroaz, 2015; Westhoff et al., 2007), mainly because it accounts for less than 2% of the heat budget (Hebert et al., 2011; Webb & Zhang, 1997). The contribution of frictional energy in the water heat balance is generally limited during summer runoff months (Webb & Zhang, 1997), and we assume this is true in the downstream Kuparuk River, which has relatively low gradient channels. We assume that T_w is homogeneous and that the water column is well mixed, which appears justified because the channels in Kuparuk River are generally small and shallow.

We postulated a constant water surface albedo over the inundation season in the simulations. However, albedo experiences some variation depending on suspended sediment concentration and more substantial changes during the breakup season when ice cover changes rapidly.

Another component that has not been included in the river water temperature model is the heat flux through infiltration in the riverbed. Hyporheic flow transfers heat into the bed sediments and as a result controls the active layer (Brosten et al., 2006). Riverbed warming may be stronger than that inferred from the simulations.

Hyporheic flow could also penetrate the deposits and alter the sedimentary structure. Water freezes to the streambed every winter (i.e., bedfast ice; Best et al., 2005). Thermal properties of the underlying sedimentary materials depend strongly on the water/ice content (Clow, 2018a). Here these are assumed to be constant without consideration of water/ice inclusion, which would cause biases for both water temperature T_w and soil temperature T_s simulations.

Uncertainties in the simulations also stem from the input parameters. Daily T_a and T_g used in the simulations differ from the site where the river discharge was measured due to the 20-km distance between the University of Alaska Fairbanks Deadhorse station and the USGS hydrologic station. The empirical constants for water surface latent heat (H_l) and riverbed heat flux (H_b) calculations are adopted from different river systems (Hebert et al., 2011; Webb & Zhang, 1997) owing to the lack of in situ measurements. Though the presented model performance is adequate, calibration and sensitivity analysis are needed to further refine the model. The meteorological observations obtained from ERA-Interim reanalysis are always much less accurate than any in situ observations. In addition, the coarse-resolution reanalysis data have lower variance and less extremes than point measurements. Possibly, the lack of accurate in situ measurements could explain some of the issues with model performance.

The CVPM is shown to be of sufficient quality in permafrost temperature simulation. However, CVPM does not appear to resolve the zero curtain, which should be considered in future studies. Lastly, equilibration of deep permafrost typically requires hundreds of years (Riseborough et al., 2008), but the observed T_g records



as employed for spinning up our simulations are limited to 8 years. It must be noted that uncertainty in the initial temperature condition has a limited effect for our analyses because we only focus on the upper several meters of the subsurface where the active layer exists and responses are more driven on annual time scales.

5.2. Model Results Versus Ground-Penetrating Radar Mapping

Streamflow provides enough input of heat into the subsurface to warm the frozen layer. River flow can prevent the development of the permafrost beneath the riverbed (Viereck, 1970, 1973). Earlier studies suggest ALT in the Kuparuk River watershed ranges from 20 cm to more than 100 cm. ALT in the floodplain is typically more than 70 cm (Nelson et al., 1997; Shiklomanov & Nelson, 1999). Detailed 3-D geometry of the permafrost beneath the Kuparuk River has been mapped by ground-penetrating radar (GPR; Bradford et al., 2005; Brosten et al., 2006, 2009). Those observations indicate rapid heat absorption and heat loss in the gravel-lined streams. Thaw depths increase to greater than 100 cm for earlier onset of inundation. Substantial and persistent flows promote subchannel thaw, resulting in a maximum thaw depth (280 cm) in September. The thaw front in the main riverbed was observed to be about 100 cm deeper than that in the riverside (Brosten et al., 2006). The simulated ALT distribution pattern in this study matches relatively well with the pattern shown from GPR measurements. The simulated thaw front reached its deepest extent in late September (Figure 6). ALT in the sand and gravel riverbed was generally more than 400 cm and can indeed be more than 100 cm deeper than the ALT in adjacent areas without river inundation (Figures 7, 8, and 12). Different thaw bulb responses to river inundation in the bare sand and gravel-dominated channel beds and organic-capped floodplain or stream profiles (Figure 9) were also clearly distinguished by the GPR measurements (Brosten et al., 2006).

5.3. Implications for the Changing Arctic

Climate change is transforming Arctic river systems. Spring snowmelt has become earlier as a result of the Arctic warming (Tan et al., 2011). River and lake ice breakup has occurred earlier at a rate of 0.65 days per decade since the 1850s (Magnuson et al., 2000). The earlier spring snowmelt and river breakup date allow more heat to penetrate into soils (Figure 11), leading to the substantial warming of the underlying permafrost. Stream geochemistry suggested that thaw bulbs beneath some Alaskan streams are seasonally and spatially increasing (Keller et al., 2010). Spring snow water equivalent is projected to increase at high latitudes (Adam et al., 2009). Discharge of large rivers in the Arctic has increased by 7% since the 1930s (Peterson et al., 2002) and increased by about 10% during 1977-2007 (Overeem & Syvitski, 2010). Continuous warming may enhance the interactions between ground and surface water and increase the groundwater discharge to rivers (Ge et al., 2011; Walvoord & Striegl, 2007). Such increasing river flow would result in longer and more extensive inundation over river floodplains (Figure 12). Together with the rising water temperatures T_w in Arctic rivers (Park et al., 2017), our experiments demonstrate that earlier and increasing inundation over the floodplain enhances the degradation of permafrost. A massive amount of old carbon is stored in Arctic floodplains (Zimov et al., 2006). A warming Arctic is likely to speed up the carbon cycle in high latitudes, and disentangling the release of terrestrial carbon requires a sound understanding of distribution of permafrost changes through the most important corridors of transport and storage, the river channel belts and floodplains (Feng et al., 2013; Kaiser et al., 2017). Our simulations suggest the downward progression of the active layer due to more sustained inundation could potentially enhance the release of the old carbon stored in the Arctic floodplains.

6. Conclusions

Driven by meteorological and hydrological observations obtained from in situ measurements and climate reanalysis data, this modeling study couples heat flux from the atmosphere into river and floodplain water and propagates it into underlying permafrost over Arctic channel belts and floodplains. We simulate water temperature T_w and permafrost soil temperatures T_s and investigate the effect of river inundation on the underlying permafrost thermal state. Our newly developed river-water thermal model and CVPM are independently validated against in situ measurements from a hydrologic station in the Kuparuk River and a permafrost monitoring station nearby, and both models show good performance.

Our model results clearly demonstrate the importance of inundation extent and timing on the permafrost thermal state in river corridors. Over the active flood season, water temperature T_w over the floodplain is



generally much higher than ground surface temperature T_g . As a result, permafrost underlying floodplains can be warmed significantly by streamflow, leading to the deepening of the active layer. In the downstream reach of the Kuparuk River, river flow results in more than a 1-m increase in ALT beneath the most active river channels. We show that permafrost temperature and ALT are sensitive to inundation timing and total annual discharge. The sedimentary characteristic of deposits in the floodplain is an additional important factor that controls the response of permafrost thermal state to streamflow. Our findings emphasize that bare sand and gravel-dominated channel or channel chutes can warm more rapidly, whereas an organic-rich top layer more typically found in floodplains dampens the downward heat flux from floodwater.

Our results imply that increasing river discharge, earlier snowmelt, and earlier river breakup in the Arctic would result in more sustained and extensive streamflow over the floodplain and hence more warming of the underlying permafrost. This is an important factor to account for in degradation of terrestrial permafrost, which could potentially lead to the release of old carbon.

Acknowledgments

Climate data were obtained from the Geophysical Institute of the University of Alaska Fairbanks (http://permafrost. gi.alaska.edu/site/dh1) and the European Centre for Medium-Range Weather Forecasts (https://apps. ecmwf.int/datasets/). We thank J. Conaway and J. Koch (USGS, Anchorage, Alaska) for discussions on the river gauging and data processing protocols. The surface elevation data set was obtained from the ArcticDEM website maintained by the Polar Geospatial Center at the University of Minnesota (https://www.pgc.umn.edu/ data/arcticdem/). The authors thank R. S. A. Anderson, S. Anderson, and A. Wlostoski (INSTAAR) for discussions on physical processes and the study site. JGR-ES reviewers and editors helped with improvement of the final manuscript. This study is funded by the U.S. National Science Foundation Office of Polar Programs Award 1503559 and the China Scholarship Council Grant 201706270140.

References

- Adam, J. C., Hamlet, A. F., & Lettenmaier, D. P. (2009). Implications of global climate change for snowmelt hydrology in the twenty-first century. *Hydrological Processes*, 23(7), 962–972. https://doi.org/10.1002/hyp.7201
- Ahmadi-Nedushan, B., St-Hilaire, A., Ouarda, T. B. M. J., Bilodeau, L., Robichaud, É., Thiémonge, N., & Bobée, B. (2007). Predicting river water temperatures using stochastic models: Case study of the Moisie River (Québec, Canada). *Hydrological Processes*, 21(1), 21–34. https://doi.org/10.1002/hyp.6353
- AMAP. (2017). Snow ice and Permafrost in the Arctic (SWIPA).
- Anderson, E. R. (1954). Energy-budget studies, water-loss investigations: Lake Hefner studies, technical report. Washington, DC: US Departement of Interior.
- Benscoter, B. W., Thompson, D. K., Waddington, J. M., Flannigan, M. D., Wotton, B. M., De Groot, W. J., & Turetsky, M. R. (2011). Interactive effects of vegetation, soil moisture and bulk density on depth of burning of thick organic soils. *International Journal of Wildland Fire*, 20(3), 418–429. https://doi.org/10.1071/WF08183
- Best, H., McNamara, J. P., & Liberty, L. (2005). Association of ice and river channel morphology determined using ground-penetrating radar in the Kuparuk River, Alaska. *Arctic, Antarctic, and Alpine Research*, 37(2), 157–162. https://doi.org/10.1657/1523-0430(2005)037[0157:AOIARC]2.0.CO;2
- Bowen, I. S. (1926). The ratio of heat losses by conduction and by evaporation from any water surface. *Physics Review*, 20(2), 823–842. https://doi.org/10.5194/hess-20-823-2016
- Bradford, J. H., McNamara, J. P., Bowden, W., & Gooseff, M. N. (2005). Measuring thaw depth beneath peat-lined arctic streams using ground-penetrating radar. *Hydrological Processes*, 19, 2689–2699. https://doi.org/10.1002/hyp.5781
- Brosten, T. R., Bradford, J. H., McNamara, J. P., Gooseff, M. N., Zarnetske, J. P., Bowden, W. B., & Johnston, M. E. (2009). Estimating 3D variation in active-layer thickness beneath arctic streams using ground-penetrating radar. *Journal of Hydrology*, 373, 479–486. https://doi.org/10.1016/j.jhydrol.2009.05.011
- Brosten, T. R., Bradford, J. H., McNamara, J. P., Zarnetske, J. P., Gooseff, M. N., & Bowden, W. B. (2006). Profiles of temporal thaw depths beneath two Arctic stream types using ground-penetrating radar. *Permafrost and Periglacial Processes*, 17, 341–355. https://doi.org/10.1002/ppp.566
- Chen, M., Rowland, J. C., Wilson, C. J., Altmann, G. L., & Brumby, S. P. (2013). The importance of natural variability in lake areas on the detection of permafrost degradation: A case study in the Yukon Flats, Alaska. *Permafrost and Periglacial Processes*, 24(3), 224–240. https://doi.org/10.1002/ppp.1783
- Chin, K. S., Lento, J., Culp, J. M., Lacelle, D., & Kokelj, S. V. (2016). Permafrost thaw and intense thermokarst activity decreases abundance of stream benthic macroinvertebrates. *Global Change Biology*, 22(8), 2715–2728. https://doi.org/10.1111/gcb.13225
- Clow, G. D. (2018a). CVPM 1.1: a flexible heat-transfer modeling system for permafrost. Geoscientific Model Development, 11, 4889–4908. https://doi.org/10.5194/gmd-11-4889-2018
- Clow, G. D. (2018b). CVPM Version 1.1 Modeling System User's Guide. Boulder: Institute of Arctic and Alpine Research, University of Colorado.
- Cohen, J., Screen, J. A., Furtado, J. C., Barlow, M., Whittleston, D., Coumou, D., et al. (2014). Recent Arctic amplification and extreme mid-latitude weather. *Nature Geoscience*, 7, 627–637. https://doi.org/10.1038/ngeo2234
- Dee, D. P., Uppala, S. M., Simmons, A. J., Berrisford, P., Poli, P., Kobayashi, S., et al. (2011). The ERA-Interim reanalysis: Configuration and performance of the data assimilation system. *Quarterly Journal of the Royal Meteorological Society*, 137, 553–597. https://doi.org/10.1002/gi.828
- Déry, S. J., Stieglitz, M., Rennermalm, Å. K., & Wood, E. F. (2005). The water budget of the Kuparuk River Basin, Alaska. *Journal of Hydrometeorology*, 6, 633–655. https://doi.org/10.1175/JHM434.1
- Evans, S. G., & Ge, S. (2017). Contrasting hydrogeologic responses to warming in permafrost and seasonally frozen ground hillslopes. Geophysical Research Letters, 44, 1803–1813. https://doi.org/10.1002/2016GL072009
- Feng, X., Vonk, J. E., Van Dongen, B. E., Gustafsson, Ö., Semiletov, I. P., Dudarev, O. V., et al. (2013). Differential mobilization of terrestrial carbon pools in Eurasian Arctic river basins. *Proceedings of the National Academy of Sciences of the United States of America*, 110, 14,168–14,173. https://doi.org/10.1073/pnas.1307031110
- Frey, K. E., & McClelland, J. W. (2009). Impacts of permafrost degradation on arctic river biogeochemistry. *Hydrological Processes*, 23, 169–182. https://doi.org/10.1002/hyp.7196
- Fritz, J. J., Meredith, D. D., & Middleton, A. C. (1980). Non-steady state bulk temperature determination for stabilization ponds. Water Research, 14(5), 413–420. https://doi.org/10.1016/0043-1354(80)90205-5
- Gao, J., & Merrick, N. P. (1996). Simulation of temperature and salinity in a fully mixed pond. *Environmental Software*, 11(1-3), 173–178. https://doi.org/10.1016/S0266-9838(96)00026-3

- Ge, S., McKenzie, J., Voss, C., & Wu, Q. (2011). Exchange of groundwater and surface-water mediated by permafrost response to seasonal and long term air temperature variation. *Geophysical Research Letters*, 38, L14402. https://doi.org/10.1029/2011GL047911
- Haine, T. W. N., Curry, B., Gerdes, R., Hansen, E., Karcher, M., Lee, C., et al. (2015). Arctic freshwater export: Status, mechanisms, and prospects. Global and Planetary Change, 125, 13–35. https://doi.org/10.1016/j.gloplacha.2014.11.013
- Hebert, C., Caissie, D., Satish, M. G., & El-Jabi, N. (2011). Study of stream temperature dynamics and corresponding heat fluxes within Miramichi River catchments (New Brunswick, Canada). Hydrological Processes, 25, 2439–2455. https://doi.org/10.1002/hyp.8021
- Hondzo, M., & Stefan, H. G. (1994). Riverbed heat conduction prediction. Water Resources Research, 30(5), 1503–1513. https://doi.org/10.1029/93WR03508
- Jarosch, A. H., & Gudmundsson, M. T. (2012). A numerical model for meltwater channel evolution in glaciers. *The Cryosphere*, 6, 493–503. https://doi.org/10.5194/tc-6-493-2012
- Jorgenson, M. T., Shur, Y. L., & Walker, H. J. (1998). Evolution of a permafrost-dominated landscape on the Colville River Delta, northern Alaska. In PERMAFROST Seventh International Conference (p. 523–529).
- Jorgenson, T. M., Harden, J., Kanevskiy, M., O'Donnell, J., Wickland, K., Ewing, S., et al. (2013). Reorganization of vegetation, hydrology and soil carbon after permafrost degradation across heterogeneous boreal landscapes. *Environmental Research Letters*, 8, 035017. https://doi.org/10.1088/1748-9326/8/3/035017
- Kaiser, K., Canedo-Oropeza, M., McMahon, R., & Amon, R. M. W. (2017). Origins and transformations of dissolved organic matter in large Arctic rivers. Scientific Reports, 7, 13064. https://doi.org/10.1038/s41598-017-12729-1
- Karlstrom, T. N. V. (1964). Surficial geology of Alaska: U.S. Geological Survey Miscellaneous Geologic Investigations Map, scale 1:1,584,000. https://doi.org/10.3133/i357
- Keller, K., Blum, J. D., & Kling, G. W. (2010). Stream geochemistry as an indicator of increasing permafrost thaw depth in an arctic watershed. *Chemical Geology*, 273, 76–81. https://doi.org/10.1016/J.CHEMGEO.2010.02.013
- King, T. V., Neilson, B. T., Overbeck, L. D., & Kane, D. L. (2016). Water temperature controls in low arctic rivers. Water Resources Research, 52, 4358–4376. https://doi.org/10.1002/2015WR017965
- Koch, J. C., Ewing, S. A., Striegl, R., & McKnight, D. M. (2013). Rapid runoff via shallow throughflow and deeper preferential flow in a boreal catchment underlain by frozen silt (Alaska, USA). *Hydrogeology Journal*, 21, 93–106. https://doi.org/10.1007/s10040-012-0934-3
- Kokelj, S. V., Lacelle, D., Lantz, T. C., Tunnicliffe, J., Malone, L., Clark, I. D., & Chin, K. S. (2013). Thawing of massive ground ice in mega slumps drives increases in stream sediment and solute flux across a range of watershed scales. *Journal of Geophysical Research: Earth Surface*, 118, 681–692. https://doi.org/10.1002/jgrf.20063
- Lachenbruch, A. H., & Marshall, B. V. (1986). Changing climate: Geothermal evidence from permafrost in the Alaskan Arctic. *Science*, 234(4777), 689–696. https://doi.org/10.1126/science.234.4777.689
- Lachenbruch, A. H., Sass, J. H., Lawver, L. A., Brewer, M. C., Marshall, B. V., Munroe, R. J., et al. (1988). Temperature and depth of permafrost on the Arctic slope of Alaska. In G. Grye (Ed.), Geology and Exploration of the National Petroleum Reserve in Alaska, 1974 to 1982, USGS Professional Paper 1399. Washington, DC: U.S. Geological Survey.
- Lachenbruch, A. H., Sass, J. H., Marshall, B. V., & Moses, T. H. (1982). Permafrost, heat flow and geothermal regime at Prudhoe Bay, Alaska. *Journal of Geophysical Research*, 87(B11), 9301–9316. https://doi.org/10.1029/JB087iB11p09301
- Lader, R., Fairbanks, A., Uma Bhatt, A. S., Walsh, J. E., Scott Rupp, T., & Bieniek, P. A. (2016). Two-meter temperature and precipitation from atmospheric reanalysis evaluated for Alaska. *Journal of Applied Meteorology and Climatology*, 55(4), 901–922. https://doi.org/ 10.1175/JAMC-D-15-0162.1
- Lamontagne-Hallé, P., McKenzie, J. M., Kurylyk, B. L., & Zipper, S. C. (2018). Changing groundwater discharge dynamics in permafrost regions. Environmental Research Letters, 13(8), 084017. https://doi.org/10.1088/1748-9326/aad404
- Li, Z., Shao, Y., Zhou, J., Tian, B., Chen, Q., & Zhang, P. (2013). Snow-depth retrieval algorithms on MEMLS. *Journal of Remote Sensing*, 17(3), 657–663.
- Ling, F. (2004). Modeling study of talik freeze-up and permafrost response under drained thaw lakes on the Alaskan Arctic Coastal Plain. Journal of Geophysical Research, 109, D01111. https://doi.org/10.1029/2003JD003886
- Magnuson, J. J., Robertson, D. M., Benson, B. J., Wynne, R. H., Livingstone, D. M., Arai, T., et al. (2000). Historical trends in lake and river ice cover in the northern hemisphere. *Science*, 289(5485), 1743–1746. https://doi.org/10.1126/science.289.5485.1743
- Matell, N., Anderson, R. S., Overeem, I., Wobus, C., Urban, F. E., & Clow, G. D. (2013). Modeling the subsurface thermal impact of Arctic thaw lakes in a warming climate. *Computational Geosciences*, 53, 69–79. https://doi.org/10.1016/J.CAGEO.2011.08.028
- McClelland, J. W., Déry, S. J., Peterson, B. J., Holmes, R. M., & Wood, E. F. (2006). A pan-arctic evaluation of changes in river discharge during the latter half of the 20th century. *Geophysical Research Letters*, 33, L06715. https://doi.org/10.1029/2006GL025753
- Mckenzie, J. M., & Voss, C. I. (2013). Permafrost thaw in a nested groundwater-flow system. *Hydrogeology Journal*, 21, 299–316. https://doi.org/10.1007/s10040-012-0942-3
- McMahon, A., & Moore, R. D. (2017). Influence of turbidity and aeration on the albedo of mountain streams. *Hydrological Processes*, 31, 4477–4491. https://doi.org/10.1002/hyp.11370
- McNamara, J. P., Kane, D. L., & Hinzman, L. D. (1998). An analysis of streamflow hydrology in the Kuparuk River Basin, Arctic Alaska: A nested watershed approach. *Journal of Hydrology*, 206(1-2), 39–57. https://doi.org/10.1016/S0022-1694(98)00083-3
- Nelson, E. F., Shiklomanov, N. I., Mueller, G. R., Hinkel, K. M., Walker, D. A., & Bockheim, J. G. (1997). Estimating active-layer thickness over a large region: Kuparuk River Basin, Alaska, U.S.A. Arctic and Alpine Research, 29(4), 367–378. https://doi.org/10.1080/00040851.1997.12003258
- Nitze, I., Grosse, G., Jones, B. M., Arp, C. D., Ulrich, M., Fedorov, A., & Veremeeva, A. (2017). Landsat-based trend analysis of lake dynamics across Northern Permafrost Regions. *Remote Sensing*, 9(7), 1–28. https://doi.org/10.3390/rs9070640
- Overeem, I., Jafarov, E., Wang, K., Schaefer, K., Stewart, S., Clow, G., et al. (2018). A modeling toolbox for permafrost landscapes. Eos, 99. https://doi.org/10.1029/2018EO105155
- Overeem, I., & Syvitski, J. P. M. (2010). Shifting discharge peaks in arctic rivers, 1977–2007. Geografiska Annaler. Series A, Physical Geography, 92, 285–296. https://doi.org/10.1111/j.1468-0459.2010.00395.x
- Park, H., Yoshikawa, Y., Yang, D., & Oshima, K. (2017). Warming Water in Arctic Terrestrial Rivers under Climate Change. *Journal of Hydrometeorology*, 18, 1983–1995. https://doi.org/10.1175/JHM-D-16-0260.1
- Pavelsky, T. M., & Zarnetske, J. P. (2017). Rapid decline in river icings detected in Arctic Alaska: Implications for a changing hydrologic cycle and river ecosystems. *Geophysical Research Letters*, 44, 3228–3235. https://doi.org/10.1002/2016GL072397
- Pekel, J.-F., Cottam, A., Gorelick, N., & Belward, A. S. (2016). High-resolution mapping of global surface water and its long-term changes. Nature, 540, 418–422. https://doi.org/10.1038/nature20584

- Peterson, B. J., Holmes, R. M., Mcclelland, J. W., Vörösmarty, C. J., Lammers, R. B., Shiklomanov, A. I., & Rahmstorf, S. (2002). Increasing river discharge to the Arctic Ocean. Science, 298(5601), 2171–2173. https://doi.org/10.1126/science.1077445
- Polyakov, I. V., Alekseev, G. V., Bekryaev, R. V., Bhatt, U., Colony, R. L., Johnson, M. A., et al. (2002). Observationally based assessment of polar amplification of global warming. Geophysical Research Letters, 29(18), 1878. https://doi.org/10.1029/2001GL011111
- Porter, C., Morin, P., Howat, I., Noh, M.-J., Bates, B., Peterman, K., et al. (2018). ArcticDEM. Harvard Dataverse. https://doi.org/10.7910/
- Riseborough, D., Shiklomanov, N., Etzelmuller, B., Gruber, S., & Marchenko, S. (2008). Recent advances in permafrost modelling. Permafrost and Periglacial Processes, 19, 137–156. https://doi.org/10.1002/ppp
- Rowland, J. C., Travis, B. J., & Wilson, C. J. (2011). The role of advective heat transport in talik development beneath lakes and ponds in discontinuous permafrost. *Geophysical Research Letters*, 38, L17504. https://doi.org/10.1029/2011GL048497
- Rudy, A. C. A., Lamoureux, S. F., Kokelj, S. V., Smith, I. R., & England, J. H. (2017). Accelerating thermokarst transforms ice-cored terrain triggering a downstream cascade to the ocean. *Geophysical Research Letters*, 44, 11,080–11,087. https://doi.org/10.1002/2017GL074912
- Serreze, M. C., & Stroeve, J. (2015). Arctic sea ice trends, variability and implications for seasonal ice forecasting. *Philosophical Transactions of the Royal Society A*, 373, 20140159. https://doi.org/10.1098/rsta.2014.0159
- Shiklomanov, N., & Nelson, F. (1999). Analytic representation of the active layer thickness field, Kuparuk River Basin, Alaska. *Ecological Modelling*, 123(2–3), 105–125. https://doi.org/10.1016/S0304-3800(99)00127-1
- Stocker, T. F., Qin, D., Plattner, G.-K., Tignor, M. M. B., Allen, S. K., Boschung, J., et al. (2013). Climate change 2013, The physical science basis, summary for policymakers.
- Streletskiy, D., Anisimov, O., & Vasiliev, A. (2015). Permafrost degradation. Snow and ice-related hazards, risks and disasters. Waltham, MA: Academic Press. https://doi.org/10.1016/B978-0-12-394849-6.00010-X
- Tan, A., Adam, J. C., & Lettenmaier, D. P. (2011). Change in spring snowmelt timing in Eurasian Arctic rivers. *Journal of Geophysical Research*, 116, D03101. https://doi.org/10.1029/2010JD014337
- Taras, B., Sturm, M., & Liston, G. E. (2002). Snow-ground interface temperatures in the Kuparuk River Basin, Arctic Alaska: Measurements and model. *Journal of Hydrometeorology*, 3(4), 377–394. https://doi.org/10.1175/1525-7541(2002)003<0377:SGITIT>2.0.CO;2
- Toffolon, M., & Piccolroaz, S. (2015). A hybrid model for river water temperature as a function of air temperature and discharge. Environmental Research Letters, 10, 114011. https://doi.org/10.1088/1748-9326/10/11/114011
- Troxler, R. W., & Thackston, E. L. (1977). Predicting the rate of warming of rivers below hydroelectric installations. *Journal Water Pollution Control Federation*, 49(8), 1902–1912.
- Viereck, L. A. (1970). Forest succession and soil development adjacent to the Chena River in Interior Alaska. Arctic and Alpine Research, 2(1), 1–26. https://doi.org/10.1080/00040851.1970.12003558
- Viereck, L. A. (1973). Ecological effects of river flooding and forest fires on permafrost in the taiga of Alaska. In *Proceedings of the Second International Permafrost Conference*, (pp. 60–67). Washington, DC: National Academy of Sciences.
- Walvoord, M. A., & Kurylyk, B. L. (2016). Hydrologic impacts of thawing permafrost—A review. Vadose Zone Journal, 15, 1–20. https://doi.org/10.2136/vzi2016.01.0010
- Walvoord, M. A., & Striegl, R. G. (2007). Increased groundwater to stream discharge from permafrost thawing in the Yukon River basin: Potential impacts on lateral export of carbon and nitrogen. *Geophysical Research Letters*, 34, L12402. https://doi.org/10.1029/2007GL030216
- Walvoord, M. A., Voss, C. I., & Wellman, T. P. (2012). Influence of permafrost distribution on groundwater flow in the context of climate-driven permafrost thaw: Example from Yukon Flats Basin, Alaska, United States. Water Resources Research, 48, W07524. https://doi.org/10.1029/2011WR011595
- Webb, B. W., & Zhang, Y. (1997). Spatial and seasonal variability in the components of the river heat budget. *Hydrological Processes*, 11(1), 79–101. https://doi.org/10.1002/(SICI)1099-1085(199701)11:1<79::AID-HYP404>3.0.CO;2-N
- Westhoff, M., Savenije, H., Luxemburg, W., Stelling, G. S., van de Giesen, N. C., Selker, J. S., et al. (2007). A distributed stream temperature model using high resolution temperature observations. *Hydrology and Earth System Sciences*, 4, 125–149. https://doi.org/10.5194/hessd-4.125-2007
- Woo, M.-K., Kane, D. L., Carey, S. K., & Yang, D. (2008). Progress in permafrost hydrology in the new millennium. *Permafrost and Periglacial Processes*, 19, 237–254. https://doi.org/10.1002/ppp.613
- Yamazaki, Y., Kubota, J., Ohata, T., Vuglinsky, V., & Mizuyama, T. (2006). Seasonal changes in runoff characteristics on a permafrost watershed in the southern mountainous region of eastern Siberia. *Hydrological Processes*, 20, 453–467. https://doi.org/10.1002/hyp.5914
- Zhang, T. (2005). Influence of the seasonal snow cover on the ground thermal regime: An overview. *Reviews of Geophysics*, 43, RG4002. https://doi.org/10.1029/2004RG000157
- Zhang, T., Barry, R. G., Knowles, K., Heginbottom, J. A., & Brown, J. (1999). Statistics and characteristics of permafrost and ground-ice distribution in the Northern Hemisphere. *Polar Geography*, 23(2), 132–154. https://doi.org/10.1080/10889379909377670
- Zhang, T., Frauenfeld, O. W., Serreze, M. C., Etringer, A., Oelke, C., McCreight, J., et al. (2005). Spatial and temporal variability in active layer thickness over the Russian Arctic drainage basin. *Journal of Geophysical Research*, 110, D16101. https://doi.org/10.1029/2004ID005642
- Zhang, T., Osterkamp, T. E., & Stamnes, K. (1996). Influence of the depth hoar layer of the seasonal snow cover on the ground thermal regime. *Water Resources Research*, 32(7), 2075–2086. https://doi.org/10.1029/96WR00996
- Zimov, S. A., Davydov, S. P., Zimova, G. M., Davydova, A. I., Schuur, E. A. G., Dutta, K., & Chapin, F. S. (2006). Permafrost carbon: Stock and decomposability of a globally significant carbon pool. Geophysical Research Letters, 33, L20502. https://doi.org/10.1029/2006GL027484